Heliyon 10 (2024) e29512

Contents lists available at ScienceDirect

Heliyon

journal homepage: www.cell.com/heliyon

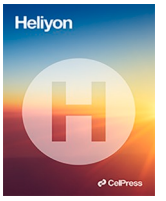

Review article

Recent progress on hard carbon and other anode materials for sodium-ion batteries

Farah Nabilah Shafiee [a,b], Siti Aminah Mohd Noor [a,b,*], Muhammad Amirul Aizat Mohd Abdah [c], Siti Hasnawati Jamal [a,b], Alinda Samsuri [a,b]

[a] Centre for Defence Foundation Studies, Universiti Pertahanan Nasional Malaysia, 57000, Kuala Lumpur, Malaysia
[b] Centre for Tropicalisation, Defence Research Institute, Universiti Pertahanan Nasional Malaysia, 57000, Kuala Lumpur, Malaysia
[c] Department of Chemistry, Faculty of Science, Universiti Teknologi Malaysia, 81310, Johor Bahru, Johor, Malaysia

A B S T R A C T

The incorporation of intermittent renewable energy sources into a consistently controlled power transmission system hinges on advancements in energy storage technologies. Sodium ion batteries (SIBs) are emerging as a primary and viable alternative material due to their electrochemical activity, presenting a potential replacement for the next generation of lithium-ion battery (LIB) energy storage materials. However, this transition may necessitate significant alterations in the anode material, given the incompatibility of the current anode with sodium ions and the electrolyte. This review provides a comprehensive summary of various anode materials employed in SIBs, categorized according to their storage mechanisms. Additionally, it explores the growing focus on utilizing hard carbon as an anode material, driven by factors such as its relatively high specific capacity compared to graphite, cost-effective production, and eco-friendly properties as it can be derived from biomass. The review further addresses recent progress in hard carbon, detailing production methods, modifications, challenges, limitations in integrating hard carbon into the anode of SIBs, and suggests potential directions for future research.

1. Introduction

Energy could be stored in the form of electrochemical, chemical, electrical, mechanical, and thermal energy.; batteries is classified as the electrochemical energy where chemical energy is converted into electrical energy through redox reaction. Batteries especially lithium-ion batteries (LIBs) with a number of interesting features such as but not limited to small ionic radius, high energy density of 120–250 Wh/kg, relatively large cell voltage, and a high conversion efficiency, have been largely used in the industry market over the past decades [1]. However, the tremendous growth rate in the demand for LIBs could significantly lead to the decreasing availability of lithium sources and therefore inevitably increasing the cost of lithium. The lithium reserves accounts for approximately 39 million tonnes [2] whereas the demand is estimated to be 240 million which is sixfold the current global reserves. Therefore, it is of paramount importance to seek alternatives to lithium to meet this urgent need despite the researchers and developers finding ways to keep availability of lithium source such as by extracting the metal from the spent LIBs [3–7].

As the electrochemical redox reaction mechanisms are similar to those found in (LIBs), sodium-ion batteries (SIBs) represent another promising technology to serve as energy storage devices for large-scale energy storage and smart grid applications. SIBs offer significant advantages over LIBs by the fact that sodium has a greater standard electrode potential (−2.71 V) than Li (−3.04 V) when compared to standard hydrogen electrode (SHE), enabling the development of high voltage SIBs ([8]; Chayambyuka et al., 2020). Furthermore, during intercalation and deintercalation, the larger ionic radius of sodium (Na^+:1.02 Å) than that of lithium (Li^+: 0.76 Å)

* Corresponding author.Centre for Defence Foundation Studies, Universiti Pertahanan Nasional Malaysia, 57000, Kuala Lumpur, Malaysia.
E-mail address: s.aminah@upnm.edu.my (S.A. Mohd Noor).

https://doi.org/10.1016/j.heliyon.2024.e29512
Received 15 March 2024; Accepted 9 April 2024
Available online 10 April 2024

results in modifications to interphase formation, phase stability, and transport parameters [9]. Recent studies reported that SIBs present a breakthrough in terms of its energy density and come with several benefits, including operation at low temperature, abundant and low cost of sodium source, great quick charging performance, and safety [10]. However, there appears to be a limited selection of suitable anodes, attributed to the higher redox potential of Na/Na^+ that eventually lowers the cell voltage of SIBs, along with the challenging for Na^+ de-intercalation due to the larger ionic radius of Na^+ (Li^+: 0.76 Å, Na^+: 1.02 Å), thus leading to the demand in exploring of anode material for SIBs. In addition, the problem of incomparable energy density of SIBs with that of LIBs (50–120 Wh/kg) still need to be addressed in order to be able to tailor and enhance the properties of SIBs [11]. Since anode acts as a site that hosts Na^+ ions which is the main indicator of ability of storing the energy, it is crucial to expedite the exploration of novel and high-performance anode materials that not only could enhance the storage, and therefore, the performance of Na-ion batteries. Moreover, the inception of green metric is also equivalently important through the utilization of environmentally friendly and economical anode materials.

To this day, there are numerous up-to-date studies on various anode materials for SIBs to compete the performance of LIBs which comprises conversion-type materials, alloying-type materials, organic materials, and carbon-based materials. Amongst the carbon-based materials, hard carbon (HC) has attracted much attention in SIBs due to their excellent characteristics such as the structure that allows higher number of Na^+ ions to be stored which delivers a high reversible specific capacity with good cycling stability [12]. The sources of environmentally friendly and low-cost HC include biomass waste materials which offer a sustainable and cost-effective solution for synthesizing HC for SIBs, aligning with principles of environmental protection and resource conservation ([13–15]; Thompson et al., 2021). Additionally, utilizing renewable sources such as sawdust and cardboard from the forestry industry provides an abundant and cheap alternative for HC production, promoting waste reduction and circular economy practices [14]. Despite that, there are still technical issues of low initial Coulombic efficiency (ICE), poor rate performance, and insufficient cycling stability to address owing to the varying irregularities of HC microstructures, as a result of the microstructures of the precursors. In light of those circumstances, there are three essential structural characteristics of HC should be emphasized: crystallinity, defects, and nanopores. These elements directly contribute to the existence of low-potential plateaus and their reversible extension. Hence, the subsequent research endeavours focused on optimizing HC's characteristics, including its synthesis process to engineer the pore structure and surface chemistry to enhance its electrochemical performance. For instance, presodiation and co-doping with heteroatoms are amongst the approaches opted for. Presodiation was carried out to compensate the irreversible sodium consumption in HC upon initial charging and discharging (Qin et al., 2023; Fang et al., 2023) and whereas doping could tune the electronic configuration to improve the HC conductivity [16]. Moreover, deeper insights into the electrochemical mechanisms governing sodium storage, diffusion kinetics, and structural evolution during charge-discharge cycles have contributed to a better understanding of its performance which could be investigated through experimental and computational modelling. Various models, including density functional theory (DFT) calculations and continuum models, have been employed to simulate Na insertion in HC at different scales [17]. Anji [18]. identified four types of Na insertion in HC, emphasizing the significance of defect sites and heteroatom doping for increasing the capacity [19]. Additionally, experimental and computational studies have demonstrated the division of sodium insertion in HC into distinct stages, providing valuable insights into the process [20]. Surta et al., presented an atomic-level understanding of the Na-binding mechanism in sodium ion batteries using Neutron total scattering data to generate structural models using pair distribution function (PDF) analysis, molecular dynamics, and reverse Monte Carlo method, and hence paving the way for precise tuning of structure-property relationships [21]. The methodologies developed in this research provide valuable insights into the analysis of amorphous functional materials and contribute to the advancement of energy storage technologies.

The proposed review aims to offer a thorough overview of recent advancements concerning HC anodes for sodium-ion batteries (SIBs), focusing on storage mechanisms, precursor materials, and preparation methods. Additionally, exploration on alternative anode materials utilized in SIBs is included to provide a broader perspective. Lastly, suggestions for enhancing the performance of HC anodes, particularly in terms of energy and power density, as well as cycling stability, were also discussed.

2. Recent progress of the development of anode materials for Na-ion batteries

The anode materials for SIBs are much more selective that they should meet the requirements stipulated to attain optimized electrochemical properties, and that include the ability to accommodate large numbers of sodium ions with good cyclability, have a similar voltage potential to that of Na metal [22], chemically stable in electrolytes, high electronic and ionic conductivity, and as above-mentioned, the material should be economical and do not pose adverse effects to the environment [23].

The anode materials can be classified as carbon-based materials, conversion-type materials, alloying-type materials, and organic materials as per their storage mechanism. The storage of Na^+ ions in the anode materials occurs based on the mechanisms of conversion reaction, alloying reaction, and intercalation.

2.1. Carbon-based materials

Despite offering high specific capacity, conversion-type and alloying type anodes are closely associated to the substantial volume fluctuations during charge/discharge, causing rapid capacity degradation and poor reversibility. On that account, carbon-based materials have become amongst the promising materials in the development of anode in SIBs for their outstanding properties that can be exploited such as physical, chemical, thermal, and electric properties. In this review, the carbon-based materials that will be discussed are hard carbon, graphite, carbon nanotubes, and graphene.

2.1.1. Hard carbon

According to Ref. [24]. hard carbon is a non-graphitized carbon where they defined the HC structure according to the "house of cards" model whereby HC has graphite-like microcrystallites in combination with amorphous regions. Such structures stem from the disordered structure that results in its short-range order as opposed to long range order of graphite as depicted in Fig. 1 [25]. Due to the structure with the interlayer spacing of 0.37–0.4 nm that allows higher number of Na^+ ions to be stored [26], HC delivers a high reversible specific capacity of approximately 300 mAh/g with good cycling stability (>100 cycles) [12]. HC is also economical and could potentially be produced in large scale [27]. In its potential profiles, the sloping region below 1.0 V is related to Na^+ ion intercalation between graphene sheets, and the following voltage intercalation reaction platform below 100 mV is induced by Na^+ ions filling in the pores. Hence, the mechanism in sodium storage is more complex in comparison to the intercalation mechanism in graphite.

2.1.1.1. Sodium storage mechanism s in HC. To date, there are six types of sodium storage mechanisms that have been proposed: (i) intercalation between graphite layers, (ii) adsorption-insertion model, iii) three stage model, iv) four stage model, v) extended adsorption-insertion model on the surface edges and defects, and (vi) adsorption-filling model [25]. The details are as follows.

i) **Insertion-filling model.** The first sodium storage mechanism, known as insertion-filling mechanism, was proposed by Dahn et al. where glucose was pyrolyzed at 1000 and 1150 °C and the resulting carbon was considered according to the "house of cards" structure model [24]. The process begins with the insertion of Na^+ ions into the interlayers of graphite microcrystals which is represented by the sloping region, followed by the accumulation of Na^+ ions into the nanovoids or micropores, from which the plateau region is formed. In situ XRD analysis is one of the techniques used to attest the theoretical explanation where Dahbi et al., confirmed the direct relationship between the slope region (from 1.2 to 0.15 V) and the graphene layer spacing (d_{002}), in accordance with the Na^+ ion intercalation, along with a positive linear relationship between the platform capacity (from 0.15 to 0.00 V) and the average micropore size [28]. In recent study, Cai et al., revealed a revised insertion-filling using time-resolved in situ XRD and time-resolved Raman to study the sodium storage mechanism. Time-resolved Raman is sensitive to the evolution of crystal and local structures. Prior research suggests that the insertion of Li^+ or Na^+ ions into the graphitic layers of HC results in the occupation of electrons in the π* antibonding band. This phenomenon weakens the C–C bonds and elongates their length, consequently causing a redshift of the G-band. During discharge within the slope region (above 0.1 V), the G-band of the spectrum progressively splits into two bands and shifts towards lower wavenumbers, reflecting the intercalation of Na^+ ions into the interlayers of graphitic carbon. Conversely, in the plateau region (below 0.1 V), the change in G-band is marginal, suggesting ongoing sodium storage through pore filling. Simultaneously, the intensity of the D-band diminishes during sodiation, potentially attributable to Na^+ adsorption occurring on the surfaces and various defects of the hard carbon nanofibers (HCNFs). On the other hand, time-resolved in-situ XRD further examined the change occurred in the interlayer spacings where the broad (002) peak becomes narrow with decreasing intensity, suggestion the formation of NaCx phase due to the Na^+ insertion.

ii) **Adsorption-insertion model.** [29]. proposed this mechanism through their study on hollow polyaniline nanowire derived HC [30]. They proposed that the mechanism of sodium storage in hard carbon was similar to that of lithium in graphite. The adsorption of Na^+ ions on the surface, defects, and pores occur in the slope region, whereas the intercalation of Na^+ ions into carbon layers occur in the low potential plateau below 0.1 V. They also found a critical minimum spacing of 0.37 nm between the graphitic layers is required to effectively facilitate Na^+ ion insertion. Kamiyama et al., et al. proposed three mechanisms for sucrose-based hard carbon: (i) defect-assisted adsorption at the edge of graphitic planes, (ii) defect-assisted insertion into graphitic layers, and (iii) insertion followed by filling of micropores resulting in pseudo-metallic clusters [12]. Mechanisms (i) and (ii) contribute to sloping region capacity (SRC), while mechanism (iii) contributes to plateau region capacity (PRC). The relative contribution of sodium ion insertion to SRC and PRC depends on factors such as carbonization or pyrolysis

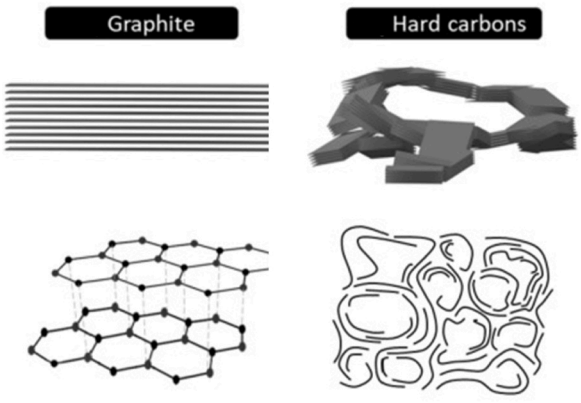

Fig. 1. The illustrated structure of hard carbon and graphite [25]. Reproduced with permission. Copyright 2022, Elsevier.

temperatures, types of surface defects/atoms, and pore characteristics in the HC [31]. corroborates this recently proposed model, wherein we conducted an analysis and comparison of the SRC and PRC contributions of samples of hard carbon microspheres (HCMS) synthesized at 600 °C. A more pronounced irreversible capacity loss is observed due to the presence of increased defects, dangling bonds/heteroatoms (H, O), and enhanced surface area compared to samples synthesized at 1000 °C. Notably, the first cycle irreversible loss for lower DEG ratio (20DEG-HCMS) surpasses that of higher DEG ratio (50DEG-HCMS) incorporated prior to the synthesis process, both at 600 °C and 1000 °C, despite the opposite trend observed in the BET surface area S_{BET} (1115 m^2/g for 20DEG-HCMS and 871 m^2/g for 50DEG-HCMS). This discrepancy underscores the role of irreversible sodium insertion into the micropores and mesopores demonstrated by 20DEG-HCMS compared to the higher volume fraction of ultra-micropores in 50DEG-HCMS.

iii) **Three stage model.** [32] proposed three stage model which is also known as adsorption-intercalation-adsorption as the model of interaction between Na^+ ions and HC. The reversible interlayer expansion of glucose-derived HC which was determined via three measurements consisted of ex-situ XRD, Raman spectroscopy, and neutron diffraction experiments, were in accordance with the adsorption-insertion model. On the other hand, the concentration of defect storage sites connected to the sloped region was obtained by neutron pair distribution function (PDF) analysis. Nevertheless, after the relatively slow values associated with the intercalation process, they discovered an increase in the sodium diffusion coefficient values near the end of the plateau region using galvanostatic intermittent titration (GITT). In conclusion, they proposed that Na-ion adsorption on pore surfaces near the edge of the plateau zone is minor. Bobyleva et al., investigated pseudocapacitive behaviour of glucose-derived HC using linear sweep voltammetry where their findings agree with the model proposed by Bommier et al., [33]. Equation $\log(i) = \log(a) + \log(b)$ was fitted linearly to produce the b-value at a fixed potential with a 5 mV step where three b-value minimums were obtained. Approximately 600–700 mV peak current is ascribed to the galvanostatic charge-discharge curve's slope area. Since the b-values in this instance fall between 0.86 and 0.94, the processes can be categorized as pseudocapacitive-dominant processes. Processes at ~600 mV can be classified as "adsorption" according to the "adsorption-intercalation" model because of their significant pseudocapacitive contribution.

iv) **Four stage model.** Alvin et al., introduced a fourth step to the three-stage model using lignin-derived HC as the subject to study. The ex situ nuclear magnetic resonance (NMR) spectra and Na^+ ion diffusion coefficients demonstrated a partial micropore filling that was shown in the sloping region between 0.2 and 0.1 V, after the adsorption of Na^+ on the high-energy surface defects and edge sites [34]. Meanwhile, below 0.1 V in the plateau region, Na^+ ions were intercalated into the graphitic layers and a secondary adsorption of sodium in the micropores was observed to occur in the region close to the cut-off potential.

v) **Extended adsorption–insertion model.** This model was presented by Sun et al. from the investigation on ginkgo leaves-derived HC produced in the pyrolysis temperatures ranging from 600 to 2500 °C [35]. From lowest to highest temperature, three types of HCs microstructures gradually appeared as summarized by Alvira et al. [25],:

1. Highly disordered carbon with d_{002} larger than 0.40 nm which is sufficient enough for Na^+ to freely transfer via a "pseudo-adsorption" mechanism that is represented by the sloping region in the capacity profile together with the defects introduced as the storage sites in the microstructure.
2. Pseudo-graphitic structure with d-spacing of 0.36–0.40 permits the interlayer intercalation and de-intercalation process, giving the low-potential plateau with a theoretical insertion capacity is 279 mAh/g corresponding to the formation of NaC_8.
3. There are some interlayer spacing that are below than 0.36 nm in the microstructure that can be challenging for intercalation and de-intercalation to occur. The optimal outcomes in terms of capacity, rate, and cyclic performance were achieved by the HC pyrolyzed at temperatures between 1200 °C and 1300 °C. In these conditions, interlayer spacings were larger than 0.40 nm, and a coexistence of interlayer dimensions ranging between 0.36 and 0.40 nm. This configuration provided enhanced storage capacities through both "pseudo-adsorption" and "interlayer insertion" mechanisms.

vi) **Adsorption-filling model.** Proposed by Zhang et al., in 2016, this model involves adsorption of Na^+ ions onto the defect sites in sloping region while filling in the nanopores in the plateau region [36]. They stated that there were no changes observed upon sodiation in polyacrylonitrile-derived carbon nanofibers at (002) peak from in situ XRD analysis. The sodium intercalation between graphene layers mechanism was eliminated from the possibility that affects the sodiation and subsequently presented the adsorption-filling mechanism. While the plateau region (below 0.1 V) is attributed to nanopore filling, the slope region (1.0–0.1 V) on the other hand is associated with sodium ion adsorption on graphene sheet surfaces. Surta et al., established the relationship between Reverse Monte Carlo (RMC) model and electrochemical properties where defect binding in the sloping region is ascribed to the deposition/stripping of sodium into crease sites, where sodium is more strongly bound. In these sites, there is a wider distribution of binding strengths, necessitating a larger voltage range to fully extract the sodium (Surta et al.., 2023). These crease sites typically consist of odd-numbered rings, mostly greater than 6-membered, pores, edges, and potentially carbonyl or carboxyl moieties. The aggregation of >6-membered rings and pores presents a synthetic targeting challenge. A characterization method aimed at identifying these features could provide valuable insights for the rational design of new hard carbon materials. While the interfacing of graphene sheets is inherent in hard carbon, increasing these features, and consequently augmenting crease sites, is crucial for modulating the sloping region's capacity. This mechanism however received some skepticism from various research groups. This mechanism explains that the specific capacities derived from the plateau region should correlate positively with the pore volume of hard carbon. However, no clear correlation has been observed. For instance, hard carbon synthesized at temperatures below 1000 °C, which possessed abundant micropores, did not exhibit any plateau capacity. This underscores the need for a more refined understanding of the micropore term, which will be discussed further in this article, particularly regarding the types of micropore interactions that truly contribute to sodium storage.

These models occur simultaneously upon the charging or sodiation process at two regions: a high-potential sloping region and a plateau within the potentials below 0.10 V as illustrated in Fig. 2 [25].

From the profiles and mechanisms behind them, it could be established that the resultant microstructure, surface area, and degree of graphitization of HC could significantly affect the way of Na^+ ion stored in HC whereby all of which are strongly varied according to the precursor of HC production, design of HC synthesis, and the temperature carbonization or pyrolysis process which will be reviewed in Section 3 and 4 [36–38].

HC is a unique material since it could be prepared from biomass-derived, synthetic polymer-based, and fossil fuel-based precursors. Numerous studies have been focusing on the utilization of HC as the anode material owing to several factors including relatively high specific capacity than that of graphite due to variation of microstructures, low-cost production and eco-friendly as they can be derived from biomass.

2.1.1.2. Resources of hard carbon. HC can be produced specifically from thermosetting-type precursors in which the precursors could not have graphite as the resultant product albeit being carbonized at high temperatures (>1000 °C). In recent study, Asfaw et al., discussed the study on the utilization of hard carbon microsphere (CMS) obtained from the synthetic polymer of polyphenols [39]. The polyphenols were synthesized from resorcinol and formaldehyde in the presence of HCl catalyst before the subsequent carbonization at different temperatures of 1200 °C, 1400 °C, and 1500 °C. CMS carbonized at 1500 °C was the most graphitized HC, as evidenced by the plasmon peaks in EELS caused by the collective oscillation of the ($\sigma+\pi$) valence electrons, which appeared in the range of 25–26 eV for the CMS samples and comparable with that of pristine graphite at 26.8 eV (Fig. 3(a)). With an ICE of 85–89 % and a reversible capacity of 300–340 mAh/g at 10 mA/g, electrochemical tests showed that the HC synthesized at 1500 °C performed best (Fig. 3(b)). Commercial alkali lignin was also used as the precursor in recent study where the lignin was subjected to heat treatment for oxidation at three different temperatures (150 °C, 200 °C, and 250 °C) to modify the crosslinking structure of the lignin prior to pyrolysis step at 1350 °C [40]. In contrast to the lignin without oxidation, the oxidized lignin was much softer and more crumble (Fig. 3(c)). The optimal pre-oxidation temperature of 200 °C led to a noticeable improvement in the performance of the hard carbon (LK-200-1350), yielding a capacity of 307 mAh/g in propylene carbonate (PC) and 336.4 mAh/g in diglyme electrolytes when charging and discharging at a rate of 25 mA/g. The dilated layer distance allows for a significantly improved rate capability, with a capacity of 235.6 mAh/g at 2000 mA/g. Furthermore, cyclic performance was found to be stable with only slight fading over 250 cycles. By using in-situ Raman to investigate the Na^+ ion storage mechanism in LK-200-1350, it is possible that the capacity was mainly contributed from the pore filling and Na^+ ion adsorption as there was no significant changes in the G and D peak upon the cycle (Fig. 3(d)).

Motivated by the high number of masks being discarded improperly, Lee et al., proposed PP-based waste disposable mask as the precursor to synthesize hard carbon. The masks were subjected to sulfuric acid treatment, followed by pyrolysis, which produced polyaromatic and carbon structures, respectively. A longer sulfuric acid treatment time resulted in a higher carbon yield (up to 50 %) by which the specific mechanism was further validated using NMR analysis, showing that sulfonation resulted in polyaromatic hydrocarbons in addition to simple cross-linking, which contributed to the distinct D and G bands in the Raman spectra. The anode with the higher carbon yield upon carbonization demonstrated a high reversible capacity of around 340 mAh/g at a current rate of 0.01 A/g

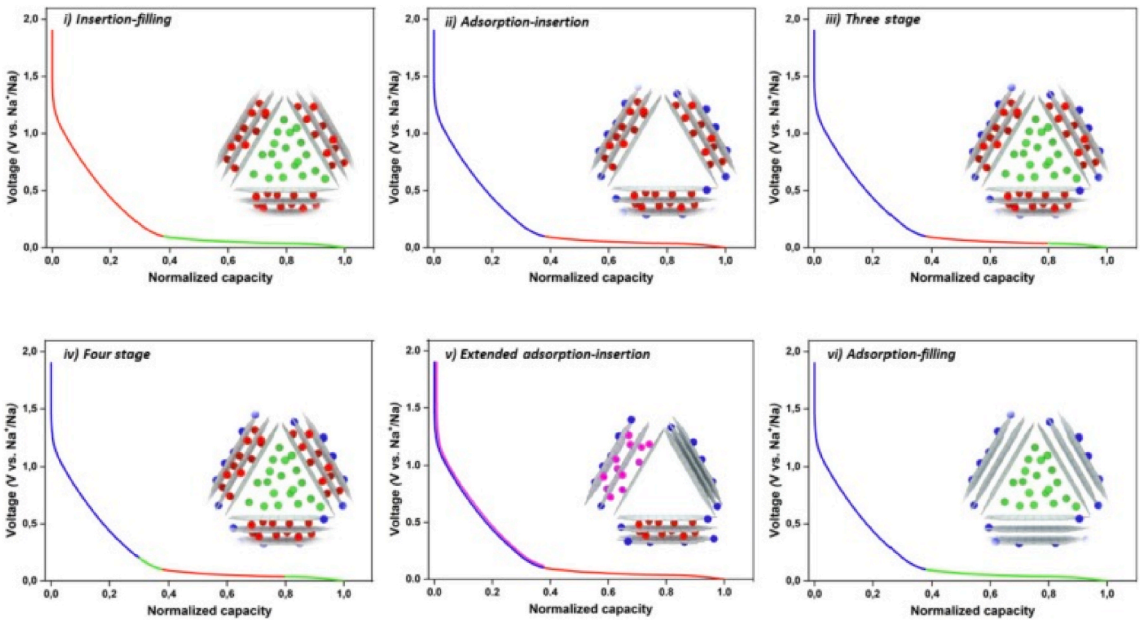

Fig. 2. Galvanostatic charge and discharge profiles of hard carbon indicating the mechanism occurred therein [25]. Reproduced with permission. Copyright 2022, Elsevier.

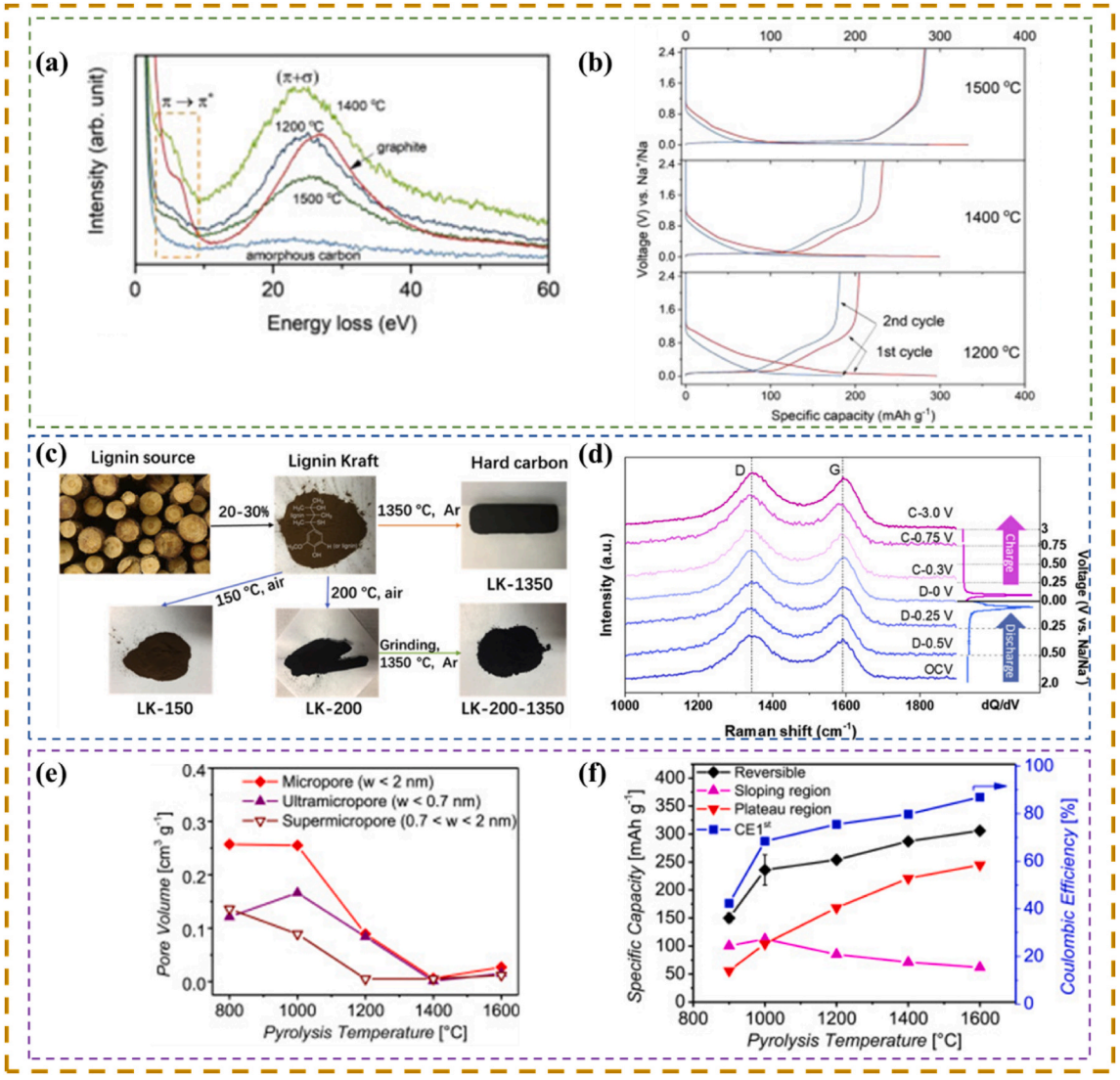

Fig. 3. (a) Low-loss EELS features in the CMS samples, amorphous carbon, and graphite references. (b) The specific capacity of CMS samples as a function of voltage vs Na^+/Na [39], (c) Hard carbon without and with grinding prior to pyrolysis. (d) Selective in-situ Raman spectra of LK-200-1350 upon charging and discharging [40]. (e) The distribution of pore sizes as a function of pyrolysis temperature. (f) The specific capacity of the synthesized hard carbon as a function of pyrolysis temperature [41]. Reproduced with permission. Copyright 2020, 2022, Elsevier.

and the capacity maintained about 53 % of the capacity at a higher current rate of 1 A/g.

While synthetic precursor could yield satisfactory performance, biomasses as precursor could also yield comparable performance as biomasses could produce variation of morphological properties. Zou et al., set up a simple scale-up procedure from lignite, which is a naturally-found carbon source, to produce inexpensive hard carbons (a-LC) [42]. The microstructure and defect of the a-LC could be tailored by varying the carbonization temperature and a variety of sodium-ion storage behaviours could be observed. With an initial Coulombic efficiency of 82 %, a-LC carbonized at 1200 °C (a-LC-1200) in particular could produce a high capacity of 256 mAh/g. Additionally, it displayed a superior rate performance of 146 mAh/g at the highest applied current rates of 20 C, respectively (1 C was defined as 200 mA/g). Meanwhile, the performance of hard carbon derived from Prunus armeniaca seed shell biomass was also investigated [43]. The material was pyrolyzed at various temperatures in order to achieve the appropriate levels of conductivity and surface area. Broad peaks at $2\Theta = 23^\circ$ and 43° in the XRD investigation indicated distinguishing characteristics of the hard carbon whereas the purity of 99.9 % was confirmed by EDX analysis. It was discovered that the CV curves of the hard carbon cells made in this work were remarkably similar to that of commercial hard carbon cells where the material pyrolyzed at 1200 °C revealed the highest capacity of 210.2 mAh/g using 0.1 A/g, and the capacity fade was determined to be 0.11 according to charge/discharge cycle measurements with constant current. [44], explored sawdust as the precursor to produce hard carbon [45]. After pyrolyzing from 1000 to 1600 °C, the sawdust pyrolyzed at 1400 °C (SC-1400) displayed the highest initial reversible capacity of 309.2 mAh/g at a current

Table 1
The electrochemical performance of HC with the precursors, pre-treatment and electrolyte used in their SIBs.

HC Precursor	Pre-treatment method	Pyrolysis temperature (°C)	Electrolyte	Half-cell electrochemical performance				Full-cell electrochemical performance						Ref
				Discharge capacity/Current density	ICE (%)	Reversible capacity/ Current density	Rate capacity (%)	Cathode	Voltage output (V)	Discharge capacity/ Current density	ICE (%)	Reversible capacity/ Current density	Rate capacity (%)	
Polyphenol	Acid catalysed sol-gel	1500	1.0 M $NaPF_6$ in EC and DEC (1:1)	332.8 mAh/g at 20 mA/g	85	227 mAh/g at 80 mA/g over 150 cycles	41 mAh/g at 1280 mA/g	Prussian white $Na_{2-x}Fe[Fe(CN)_6]$	2.7–3.5	156 mAh/g at 20 mA/g	~95	~100 mAh/g at 20 mA/g over 50 cycles	–	Asfaw wet al., 2020
Alkali lignin	Oxidation at 150, 200 and 250 °C	1350	1.0 M $NaPF_6$ in diglyme	400 mAh/g at 25 mA/g	81.4	288 mAh/g at 200 mA/g over 250 cycles	236 mAh/g at 2000 mA/g	–	–	–	–	–	–	[40]
Poly (aniline-*co*-pyrrole)	Template assisted followed by acid wash after pyrolysis	1000	1.0 M $NaPF_6$ in EC and DEC (1:1)	~900 mAh/g at 0.1 A/g	~30	~324.0 at 0.1 A over 300 cycles	169.8 mAh/g at 5.0 A/g	Prussian blue	2.0–3.0	~125 mAh/g at 100 mA/g	~98	127.8 mAh/g at 100 mA/g over 100 cycles	74 mAh/g at 500 mA/g	[16]
Disposable polypropylene mask	Activation using H_2SO_4	1600	1 M $NaPF_6$/in DEGDME	~440 mAh/g at 0.01 A/g	68	~165 mAh/g at 1 A/g over 100 cycles	~165 mAh/g at 1 A/g	–	–	–	–	–	–	[74]
Sucrose and phenol formaldehyde resin	Pre-carbonization in vacuum at 200 °C	1300	0.8 M $NaPF_6$ in EC and DMC	369 mAh/g at 20 mA/g	85	287 mAh/g at 20 mA/g over 100 cycles	N/A	–	–	–	–	–	–	[35]
Phenolic resin	N/A	1300	0.8 M $NaPF_6$ in EC and DMC	413.3 mAh/g at 30 mA/g	72	~260 mAh/g at 50 mA/g over 100 cycles	~50 mAh/g at 2000 mA/g	–	–	–	–	–	–	[47]
D-glucose	Pre-carbonization in vacuum at 220 °C	1100	1 M $NaClO_4$ in EC and DEC (1:1, v/v), and with 2 % FEC	394 mAh/g at 50 mA/g	78	160 mAh/g at 0.5 A/g over 300 cycles	97 mAh/g at 1 A/g	–	–	–	–	–	–	[75]
Cork	Oxidation at 300 °C	1500	1.0 M $NaPF_6$ in EC and DEC (1:1)	~320 mAh/g at 20 mA/g	~88	250 mAh/g at 20 mA/g over 100 cycles	~60 mAh/g at 1000 mA/g	Prussian white $Na_{2-x}Fe[Fe(CN)_6]$	2.75–3.75	152 mAh/g at 32 mA/g	90	129 mAh/g at 32 mA/g over 20 cycles	~80 mAh/g at 160 mA/g	[76]
Ganoderma spores	Vacuum drying at 110 °C	700	1.0 M $NaClO_4$ in EC and DMC (1:1) with 5 wt% FEC	843 mAh/g at 0.05 A/g	43	300 mAh/g at 0.05 A/g 165 mAh/g at 2 A/g over 10000 cycles	211 mAh/g at 1 A/g	$Na_3V_2(PO_4)_3$	2.5–3.0	~96 mAh/g at 0.1 A	~97	94 mAh/g at 0.1 A over 200 cycles	N/A	[55]
Sawdust	Vacuum drying at multi stages from 120 to 800 °C	1400	1.0 M $NaClO_4$ in EC, DMC, EMC (1:1:1)	~360 mAh/g at 30 mA/g	83.4	296 mAh/g at 30 mA/g over 100 cycles	73.4 mAh/g at 600 mA/g	$Na_3V_2(PO_4)_2O_2F$	3.75–4.25	~440 mAh/g at 60 mA/g	62.7	219.6 mAh/g at 60 mA/g over 10 cycles	–	[45]
Waste hemp cannabis	Low temperature pyrolysis followed by activation using K_2CO_3	700, 800	1 M $NaC_2F_6NO_4S_2$ in DMC and EC (1:1)	359.5 mAh/g at 0.03 A/g	73	~50 mAh/g at 2 A/g over 300 cycles	79 mAh/g at 1 A/g	–	–	–	–	–	–	Antoran et al., 2023
Hazelnut shell	Activation using HCl	1400	1 M $NaPF_6$/EC + DMC	375 mAh/g at 20 mA/g	91	306 mAh/g at 20 mA/g over 100 cycles	100 mAh/g at 500 mA/g	–	–	–	–	–	–	[55]
Green tea leaves	Activation using HCl	1400	1 M $NaClO_4$ in EC and DEC (1:1, v/v)	~410 mAh/g at 30 mA/g (0.1C)	69	173.7 mAh/g at 60 mA/g	67.3 mAh/g at 600 mA/g (2C)	–	–	–	–	–	–	Pei et al., 2020

(*continued on next page*)

Table 1 (*continued*)

HC Precursor	Pre-treatment method	Pyrolysis temperature (°C)	Electrolyte	Half-cell electrochemical performance				Full-cell electrochemical performance						Ref
				Discharge capacity/Current density	ICE (%)	Reversible capacity/ Current density	Rate capacity (%)	Cathode	Voltage output (V)	Discharge capacity/ Current density	ICE (%)	Reversible capacity/ Current density	Rate capacity (%)	
						(0.2C) over 200 cycles								
Fungus pre-treated basswood	Pre-carbonization in vacuum at 300 °C	1300	1 M $NaPF_6$ in diethylene glycol dimethyl ether	329 mAh/g at 10 mA/g	88.2	291.0 mAh/g at 10 mA/g	100 mAh/g at 400 mA/g	P2–$Na_{2/3}Ni_{1/3}Mn_{1/3}Ti_{1/3}O_2$ (NaNMT)	3.25–3.5	274.0 mAh/g at 20 mA/g	71.5	193.4 mAh/g at 20 mA/g over 100 cycles		[45]
						~221 mAh/g at 200 mA/g over 536 cycles		–	–	–	–	–	–	
Bagasse	Dried at 80 °C	900	1 mol/L $NaClO_4$ in EC and DEC (1:1, v/v)	589.3 mAh/g at 0.2C	55	~270 mAh/g at 0.2C over 200 cycles	N/A	–	–	–	–	–	–	Wang et al., 2021
				288 mAh/g at 10C	63	~120 mAh/g at 10C over 800 cycles		–	–	–	–	–	–	
Prunus armeniaca seed	Dried at 105 °C	1200	1 M $NaClO_4$ in PC and EC	~185 mAh/g at 0.3 A/g	~95	~160 mAh/g at 0.3 A/g over 100 cycles	~85 mAh/g at 1 A/g	–	–	–	–	–	–	[43]
Peanut shell	Hydrothermal in NaOH solution	800	1 M $NaClO_4$ in EC and PC (1:1)	466 mAh/g at 30 mA/g	58	256 mAh/g at 30 mA/g over 100 cycles	100 mAh/g at 1500 mA/g	–	–	–	–	–	–	[54]
Hazelnut shell	Hydrothermal in H_2SO solution	1000	1 M $NaClO_4$ in EC and PC	404 mAh/g at 37.2 mA/g	55.6	232 mAh/g at 37.2 mA/g over 100 cycles	N/A	–	–	–	–	–	–	[77]
Sunflower seed shells Spent coffee ground Rose stems	Hydrothermal in water	1200	1.0 M $NaPF_6$ in EC and DMC (1:1)	376.40 mAh/g at 24.8 mA/g * Sunflower seed shells exhibited the best performance	76	120 mAh/g at 372 mA/g over 1000 cycles	~170 mAh/g at 372 mA/g	–	–	–	–	–	–	[78]
Onion peel (OP)	OP mixed with Na_2HPO_4	750	1 M $NaClO_4$ in EC and DEC (1:1)	1728.7 mAh/g at 50 mA/g	23	~300 mAh/g at 50 mA/g over 40 cycles	69.4 mAh/g at 10 A/g	–	–	–	–	–	–	Sun et al., 2022

density of 30 mA/g with a high capacity retention of 95.8 % after 100 cycles in the half-cell. The HC-derived sawdust also revealed promising full-cell performance when tested with $Na_3V_2(PO_4)_2O_2F$ cathode with initial discharge capacity of ~440 mAh/g and reversible capacity of 219.6 mAh/g over 10 cycles at a current density of 60 mA/g SC-1400 showed small specific surface area, reasonable microporous structure, and large interlayer spacing.

Waste hemp hurd has been widely studied for different applications such as CO_2 absorption, additives in biocomposites, ultraviolet shielding film, and bioplastics [46–49]. In recent study, this material was also exploited for the hard carbon production where the end product was derived through the process of low temperature pyrolysis at 500 °C, followed by mild chemical activation of the resulting char through wet impregnation with K_2CO_3, and subsequent heating of the solid phase up to 700 or 800 °C under nitrogen [50]. The hard carbon activated at a char-K_2CO_3 with mass ratio of 1:4 with subsequent pyrolysis at 800 °C demonstrated the best electrochemical performance, exhibiting an excellent initial coulombic efficiency of 73 % and achieving reversible charge capacities of 267 and 79 mAh/g at 0.03 and 1 A/g, respectively. At a current density of 2 A/g, this material also displayed outstanding cyclic stability and rate capability, retaining 96 % of its capacity after 300 cycles. The structural and textural characteristics of the hard carbon, which include moderate interconnected microporosity (with pore sizes below 1 nm), a suitable concentration of defects in the carbon structure, comparatively large interplanar distances, and a specific number of closed pores, may be responsible for this more than satisfactory performance [51]. explored the utilization of sycamore fruit seeds to be derived as low-cost hard carbon to serve as an anode for SIBs through simple pyrolysis at various temperatures [52]. The reversible specific capacity of sycamore fruit seed carbonized at 1100 °C could reach 323 mAh/g at the current density of 0.1 C with the reversible specific capacity is 246.9 mAh/g when cycled at 0.4 C, and after 300 cycles, capacity retention is 87.85 %. Although the various interlayer spacings ($d_{002} \geq 0.37$ nm) of the produced hard carbon's graphite crystallites are advantageous for Na^+ ions storage, the lower d_{002} restricted the diffusion of Na^+ ions, which has an impact on their cycle stability.

The hemicellulose and cellulose content are also crucial factor to be considered regarding the production of hard carbon. Arie et al., highlighted the use of porous carbon precursor for anode materials in SIB from discarded tea leaves for their high content of hemicellulose and cellulose by employing three straightforward procedures, including direct carbonization, hydrothermal carbonization, and a combination of hydrothermal and pyrolysis carbonization [53]. The best hard carbon electrode was synthesized via the combination of methods, achieving the first discharge capacities of up to 363 mAh/g and stable cycle profiles with high discharge capacities of 179 mAh/g after 100 cycles at a current density of 100 mA/g. The large interlayer spacing, distinctive shape, and high degree of disordered carbon could provide more active sites for sodium storage and diffusion. Meanwhile, Ren et al., employed the similar combination technique to create lath-shaped hard carbon materials made from peanut shells [54]. The first phase to produce peanut shell derived hard carbon (PSDHC) was a hydrothermal pre-treatment for various treatment times, and the second was a carbonized procedure at 800 °C. The PSDHCs-4 electrode (hydrothermal treatment for 4 h) has the maximum reversible capacity of 256 5 mAh/g, and it also generated the best capacity retention at a current rate of 0.1 C after 100 cycles. More importantly, the PSDHCs-4 electrode exhibited exceptional rate performances with reversible capacities of 100 mAh/g at the highest current rates applied (5.0 C), respectively.

Song et al., used corncob as the raw material for hard carbon synthesis due the abundance of the by-product, which was pyrolyzed at temperatures between 1000 and 1600 °C [16]. The number of graphite microcrystal layers grows, the long-range order degree rises, and the pore structure exhibited a bigger size and wide distribution when the pyrolysis temperature climbs from 1000 °C to 1400 °C, resulting in the improved rate performance, initial coulomb efficiency, and specific capacity of hard carbon materials. However, the graphite-like layer started to curl as the pyrolysis temperature increased to 1600 °C, and there are fewer layers of graphite microcrystals overall, degrading the overall hard carbon material's electrochemical performance.

Some issues regarding the precursors for hard carbon such as exist in bulk causes difficulty in the fragmentation of sample, and as such bringing about the investigation of Ganoderma spores [55]. Ganoderma spores exist in the form of powder, making it easily workable as the precursor. After underwent the pyrolysis at 600 °C (NG-600), 700 °C (NG-700), 800 °C (NG-800) and 1200 °C (NG-1200), NG-700 exhibited the best performance, sustaining a reversible capacity of 165 mAh/g in sodium-ion half-cells for 10,000 cycles at 2 A/g. When combined with $Na_3V_2(PO_4)_3$ cathodes, the NG-700 anode in sodium-ion full cells could maintain its 94 mAh/g for 200 cycles at 0.1 A each cycle. The electrode's capacity retention rate is 50 % when exposed to harsh environmental conditions (~25 °C).

There are also biomasses that could be extracted for its polymeric content. For instance, Tonnoir et al., investigated the performance of hard carbon derived from tannin as the biosource of polyphenolic molecules [41]. The BET area decreased with increasing pyrolysis temperature from which the distribution of pore size comprised of micropore, ultramicropore, and supermicropore corresponding to pore volume were derived as presented in Fig. 3(e). The decrease in pore volume amount to increase in the ultramicropore which is the mainly present in the hard carbon of 1600 °C (HC1600), yielding first-cycle coulombic efficiency (CE) of 87 % and with the exception for sloping region, highest reversible capacity of 306 mAh/g, capacity at plateau region, and CE at C/20 (Fig. 3(f)). The use of precursor from different kinds of sources shows the wide range of options being offered to produce hard carbon accompanied with varieties of microstructures.

While numerous researches are focusing on the half-cell metric, it is important to showcase the performance through full cell evaluation as half-cell configuration does not necessarily construe the ability of the synthesized HC to store Na^+ ions. It was reported by Ref. [56] using macademia shell derived HC that the HC achieved a highly competitive sodium-matched full-cell utilizing a HC anode, demonstrating an impressive energy density of 186 Wh/kg at 1 C and maintaining a capacity retention of 70 % after 1300 cycles [57]. This finding was later proven that under a higher demanding rate of 5 C, the full-cell employing poplar wood-derived HC managed to exhibit prolonged cyclability of 1200 cycle [58]. Surprisingly, HC occasionally failed to make a strong impression upon the assessment using conventional half-cell testing metrics It was later discovered that in half cells, the sodium metal counter-electrode

introduces substantial impedance, often resulting in an overly pessimistic assessment of half-cell performance. This tendency undermines the recognition of the low-lying plateau part of hard carbon's capacity [57,59]. In a more recent year study [44], reported that using derivative of $Na_3V_2(PO_4)_3$ (NVP) namely $Na_3V_2(PO_4)_2F_3$ as the cathode and their rice husk-derived HC as the anode in the full-cell exhibited a reversible capacity of 258 mAh/g with an output voltage of 3.4 V, resulting in an energy density of 185 Wh/kg [60]. Despite its moderate reversible capacity of ~146 mAh/g at 0.2 A/g current density after 100 cycles in half-cell, by using NVP as cathode with lychee seed-derived HC in a full-cell test, the cell demonstrated a discharge capacity of around 266 mAh/g while maintaining approximately 91 % of its initial capacity after the 50th cycle testing at 0.1 A/g. Moreover, it exhibited a noteworthy energy density of approximately 380 Wh/kg in the region of approximately 2 V [61]. Study by Gu et al., revealed a significantly high energy density of 326.8 Wh/kg at 5C when coupling the high-entropy $Na_3V_{1.9}(Ca,Mg,Al,Cr,Mn)_{0.1}(PO_4)_2F_3$ (HE-NVPF) cathode with a hard carbon (HC) anode derived from sunflower seed [62]. Therefore, the ability of synthesized HCs to be utilized as anode are attested through these promising findings.

In general, synthetic precursors require higher pyrolysis temperatures compared to biomass counterparts when subjected to pre-carbonization and pre-oxidation prior to pyrolysis or one-step pyrolysis, which can be attributed to their decomposition temperature. To synthesize high-purity hard carbon (HC), the compounds need to fully decompose. For example, HC synthesized from polypropylene masks required temperatures of at least 1600 °C, even after acid treatment before pyrolysis, whereas biomass precursors can be pyrolyzed at relatively lower temperatures. Corncobs, for instance, yielded optimal performance after pyrolysis at 1400 °C, while ganoderma spores achieved optimum performance after pyrolysis at only 700 °C. Different biomass resources can yield varied electrochemical performance due to differences in precursor microstructure and chemical compositions. Moreover, pretreatment methods, such as hydrothermal reactions, pre-carbonization, pre-oxidation, template-assisted methods, field-assisted methods, and chemical treatments employed to optimize HC conditions, can result in microstructural properties that affect the intercalation of Na + ions into HC structures. These design and preparation methods for HC will be discussed in the next section.

2.1.1.3. Design and preparation strategies to synthesize hard carbon. Cutting-edge research in anode materials for sodium-ion batteries is predominantly focused on hard carbon due to its promising characteristics such as high capacity, low cost, and abundance. Material design strategies are aimed at addressing the key challenges associated with hard carbon, including irreversible capacity loss, sluggish kinetics, and poor cycling stability.

One aspect of material design involves tailoring the microstructure and surface chemistry of hard carbon to enhance its sodium-ion storage properties. Researchers are exploring various synthesis methods, such as templating, pyrolysis of organic precursors, and ball-milling, to control the morphology, porosity, and defect structure of hard carbon materials. These approaches aim to create a hierarchical pore structure, increase active sites for sodium-ion adsorption, and optimize the surface chemistry to facilitate reversible ion insertion/extraction processes. This includes surface functionalization and heteroatom doping to modify the chemical composition of hard carbon and improve its electrochemical performance. Introducing heteroatoms like nitrogen, sulfur, or phosphorus can create additional redox-active sites and modify the electronic structure of hard carbon, leading to enhanced sodium-ion storage capacity and cycling stability. These approaches are included in the following discussion.

Pyrolysis is basically the main method to prepare a hard carbon. Pyrolysis, or thermolysis, could be defined as an irreversible thermochemical treatment process subjected to solid or fluid chemical substances at elevated temperatures in an inert or oxygen-free atmosphere, resulting in decomposition of the matter. During pyrolysis the molecules are subjected to very high temperatures which is commonly over 1000 °C. This would lead to very high molecular vibrations at which the molecules are stretched and vibrated to a degree, allowing the decomposition to occur in which the molecules are broken down into smaller molecules.

The yield along with the characteristics from the process is dependent on the physical and chemical characteristics of the precursor and the pyrolysis parameters namely the rate of pyrolysis, temperature, and residence time [63]. For pyrolysis, temperature is mainly attributed to the significant different in the electrochemical performance due to the change in the microstructure whereas heating rate and residence time are the conditions that specifically lead to maximum solid product yield [64,65].

While it is common to control the parameter upon pyrolysis process itself, the pre-treatments employed on the precursor prior to pyrolysis could also vary the morphological properties, and therefore the overall electrochemical performance. Pre-treatments are sometimes employed due to the change in the physical and chemical properties of the precursors upon the process that could considerably affect the electrochemical performance of the synthesized hard carbon. This could be achieved via physical and chemical treatments. Physical treatment includes application of thermal energy and pressure upon the process, for instance the process involving one-step pyrolysis, hydrothermal reaction, pre-carbonization, template-assisted synthesis, and field-assisted synthesis. Meanwhile, chemical treatments involve chemical activation on the precursor prior to pyrolysis or the synthesized HC after pyrolysis.

Hydrothermal treatment process was one of the most common thermochemical processes using liquid as the medium that takes place within the temperatures from 180 to 300 °C in a closed system under autogenous pressure to ensure the liquid state of the medium is remained. Hydrothermal is usually employed prior to pyrolysis to remove volatile oxygen-rich compounds primarily as CO_2 from the precursor structure while leaving more stable carbon particles content through the five reaction mechanisms are hydrolysis, dehydration, decarboxylation, aromatization, and condensation polymerization [66]. Apart from not requiring drying step before the subsequent pyrolysis, this method is essential to the morphological transformation of the precursor into the resultant hard carbon at lower carbonization temperatures since hydrothermal produces biochar as the resultant product, offering great potential for the improvement of SIBs performance thereof. This method was exploited by Ref. [67], using reed straw (RS) as the precursor where the samples underwent hydrothermal process at 200 °C for 24 h prior to pyrolysis in a N_2 atmosphere for high SIBs performance. The hydrothermal process contributed to samples with micronic blocks homogeneously coated with nanospheres that caused the formation

of holes and channels for electrolyte to penetrate. Carbonization at 1300 °C has an exceptionally high reversible capacity of 372.0 mAh/g, along with exceptional cycling stability and an initial coulombic efficiency of 77.03 %. Ren et al., employed a two-step technique of hydrothermal in 2 M NaOH solution at 165 °C and subsequent low temperature pyrolysis to create peanut shell derived hard carbon (PSDHC) with lath shape microstructure to improve the rate capability [54]. The hydrothermal pre-treatment was carried out for various treatment times (2, 4, and 6 h), followed by carbonization at 800 °C at 10 °C/min. The HC that underwent hydrothermal pre-treatment showed ordered and parallel array of crosslinking strip in contrast to three-dimensional connected porous structure, improving the Na^+ adsorption sites and shorten the sodium ion transport route, and thus resulting in relatively high reversible capacity of 100 mAh/g at 5.0 C (1500 mA/g). Similarly, in order to produce HC with economical and feasible process, Canbaz et al., used acid solution in the hydrothermal treatment of hazelnut shell by adding 2 drops of H_2SO_4 into distilled water, followed by pyrolysis at 500, 750, and 1000 °C. The highest electrochemical properties were exhibited by HC of 1000 °C electrode fabricated using sodium alginate binder with reversible capacity of 232 mAh/g after 100 cycles at 0.1 C (37.2 mA/g) (1 C = 372 mA/g) with ICE of 55.6 %. Meanwhile, Nieto et al., employed hydrothermal to improve the electrochemical performance of biowaste-derived HC using three different biomass precursors: spent coffee ground, sunflower seed shells, and rose stems. Again, the capacity of precursor that underwent hydrothermal reaction have improved capacities and longer cyclability as the inorganic species was successfully eliminated as opposed to the ones without the pre-treatment. HC synthesized from sunflower seed shells produced a reversible capacity of 120 mAh/g over 1000 cycles at 372 mA/g.

Pre-carbonize and pre-oxidation are also another most common method used for the synthesis of HC. Both methods can be deemed as facile treatment as they do not require any chemicals or solution as a medium; the materials are directly subjected to heat treatment in vacuum, gas flow, or in ambient condition. Asfaw et al., strategized the production of hard carbon nanosheets (HCNS) from 300 °C oxidized cork. The initial coulombic efficiency (ICE) increases from 72 % at 1000 °C to 88 % at 1500 °C due to the decrease in surface area, as result of the effect of synthesis temperature. An ICE of around 88 % was reported for a reversible capacity of 276 mAh/g in a galvanostatic test conducted at 20 mA/g and ~25 °C. Although the ICE (~86 % at 30 °C and ~81 % at 55 °C) was marginally lowered, increasing the cycle temperature improved the rate performance. The reversible capacities at 30 °C and 55 °C are approximately 260 and 270 mAh/g, respectively, at 20 mA/g. In testing using constant current constant voltage (CCCV) at 30 °C, reversible capacities ranging from 237 to 242 mAh/g could be obtained at 1000 mA/g. The respective capacities obtained at 55 °C are about 234–265 mAh/g at 1000 mA/g. The applicability of the HCNS electrodes was eventually evaluated in full-cells with Prussian white cathodes, for which a discharge capacity of 152 mAh/g was obtained with the ICE of ~90 %. [44], pre-treated basswood in two-steps treatment where firstly the basswood was fungal-pre-treated and subsequently pre-carbonized at 300 C in argon flow. The hard carbon electrode from fungus-pre-treated basswood has better rate capability (242.3 mAh/g at 200 mA/g), cycling stability (93.9 % of capacity retention after 200 cycles at 40 mA/g), and increased ICE (84.3 %–88.2 %) when compared to the hard carbon electrode derived from basswood. The full cell consisted of P2–$Na_{2/3}Ni_{1/3}Mn_{1/3}Ti_{1/3}O_2$ (NaNMT) as the cathode and fungal-pre-treated basswood pyrolyzed at 1300 °C demonstrated a good reversible charge/discharge capacity of 147.3/145.8 mAh/g at 100 mA/g and maintained high specific capacity retention of 70.6 % after testing over 100 cycles.

Template-assisted method has also become an interest to be used to pre-treat the precursor of hard carbon. As the name suggests, the material for this method which could be inorganic or organic acts as a size-modulable template to tune the surface area and pore structure. The method rather simple where the materials are directly mixed with the precursor prior to pyrolysis, followed by washing thereafter. For instance, Kamiyama et al., produced superior hard carbon for Na-ion batteries by heating a freeze-dried blend of glucose and magnesium gluconate using a MgO-template method [68]. The mixture was pre-treated at 600 °C to form a carbon matrix containing nano-sized MgO particles. The carbonization of MgO by acid leaching results in hard carbon that has an incredibly high reversible capacity of 478 mAh/g and a high Coulombic efficiency of 88 % at the first cycle. Guo et al., proposed a straightforward but effective manufacturing technique for "egg puff"-like hard carbon with minimal N doping that used rosin as a precursor by simultaneous activation of potassium hydroxide and liquid salt template assistance [69]. Based on the absorption process of rapid charge transfer, the as-synthesized HC exhibited excellent electrochemical characteristics in the ether-based electrolyte, particularly at high rates. The optimized hard carbon showed an ultra-long cycle stability of reversible discharge capacity of 151 mAh/g with 12,000 cycles at 5 A/g, with an average coulombic efficiency of ≈99 % and the decay of 0.0026 % per cycle. It also displayed a high specific capacity of 367 mAh/g at 0.05 A/g and 92.9 % initial coulombic efficiency (ICE), with the capability of maintaining its high capacity of 183 mAh/g at 10 A/g. In a different study, Sun et al., incorporated disodium hydrogen phosphate, Na_2HPO_4, a novel food additive, as the

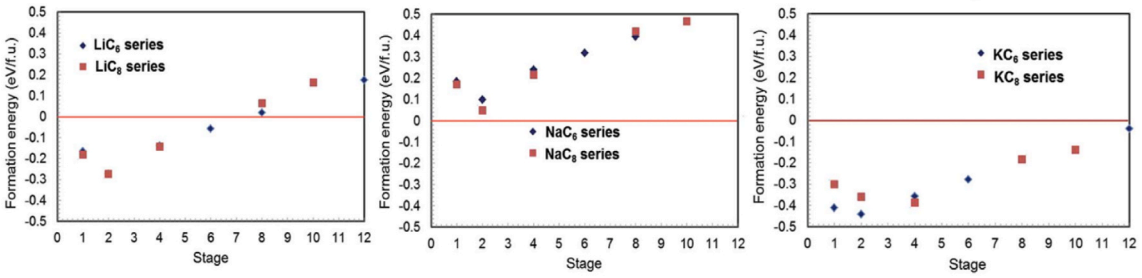

Fig. 4. The energy formation of graphite intercalated compound of alkali metal (AM-GIC) where AM are Li, Na and K metals as a function of AMC_6 and AMC_8 [79]. Reproduced with permission. Copyright 2017, Elsevier.

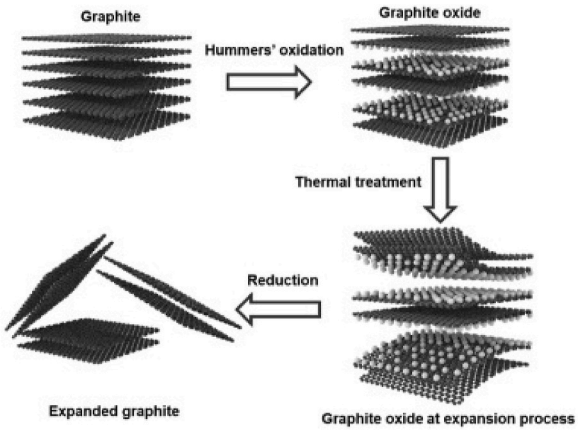

Fig. 5. The step of oxidation-reduction to obtain expanded graphite [81]. Reproduced with permission. Copyright 2021, Elsevier.

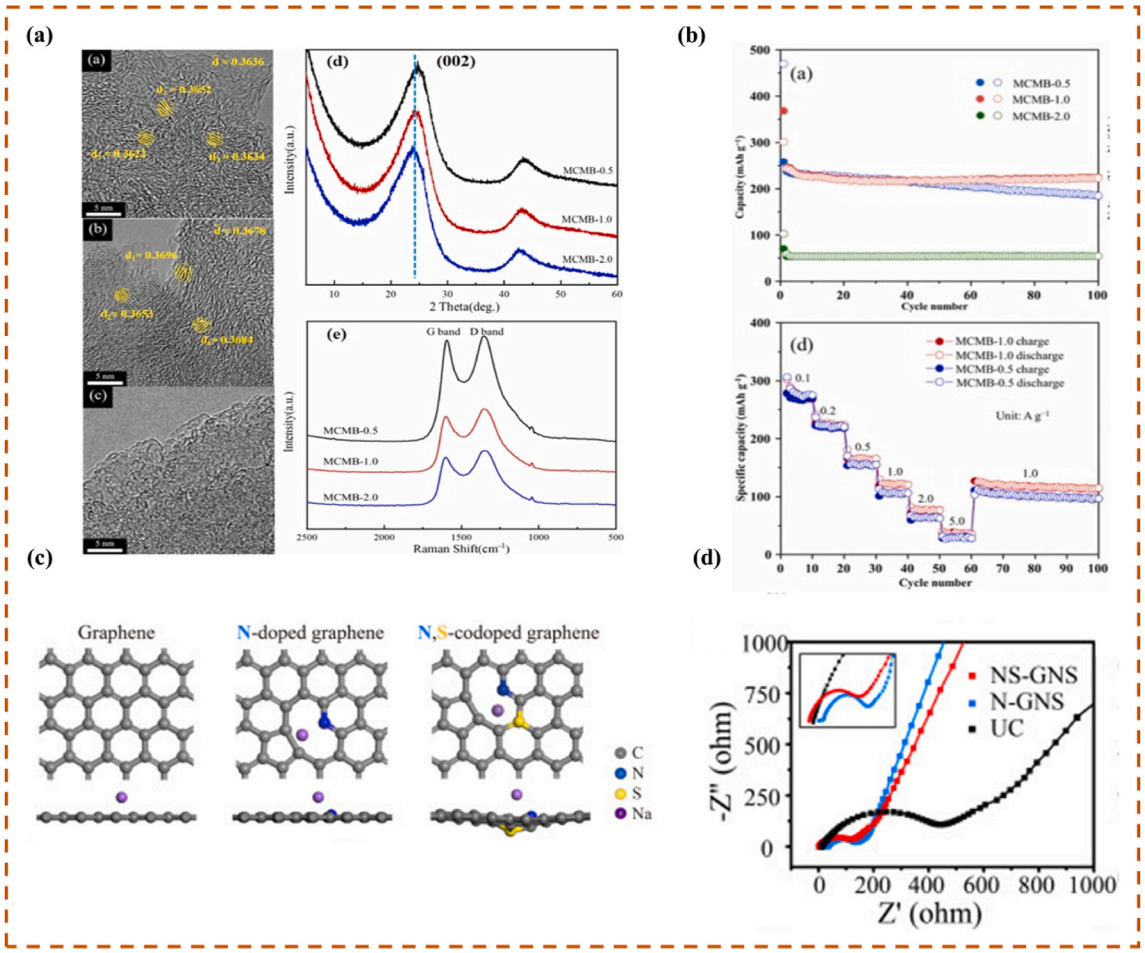

Fig. 6. (a) TEM images, the XRD and Raman spectra showing the increase in interlayer spacing from the increase in functionalized graphene (FNG) ratio and (b) the electrochemical performance with increasing amount of FNG, the electrochemical performance with increasing amount of FNG [93] (c) Adsorption energy of sodium electrochemically adsorbed onto the surface of the pristine graphene, N-doped, and N, S-codoped graphene, along with corresponding geometry configurations (d) the EIS of the UC, N-GNS, and NS-GNS [94]. Reproduced with permission. Copyright 2018, 2023 Elsevier.

template to tailor the porosity and the same time introduce heteroatom doping in onion peel biomass-derived HC (HPCN) (Sun et al., 2022). Despite its high initial discharge capacity of 1728 mAh/g, the charge capacity quickly dropped to 393.1 mAh/g at 50 mA/g, giving a low ICE of 23 %. This could be attributed to a very high surface area of 756.5 m^2/g of HPCN in comparison to the HC synthesized from direct pyrolysis at 750 °C which resulted in the high consumption of electrolyte for SEI layer formation. However, the long cyclability of HPCN could be observed with capacity retention of approximately 92 % when measured for 1000 cycles at 10 A/g.

A field-assisted sintering process of the spark plasma sintering (SPS) method was used to synthesize HCs from various carbon sources [70]. This emerging technology cannot only prepare HC at a high rate of speed compared with traditional sintering routes but also effectively boost the pyrolysis process, leading to the formation of HCs with fewer defects and smaller surface areas. Moreover, the accelerated pyrolysis mechanism was revealed by molecular dynamics simulations. As a result, HC made from the SPS method exhibits a significantly enhanced sodium storage capacity and kinetics.

Apart from physical treatment, chemical treatment could also be employed upon pre-treatment or post-treatment. Chemical treatment could be carried out to remove inorganic impurities prior or post to subjecting the sample to pyrolysis step, as an activation agent to introduce functional groups or as a way to dope heteroatoms into HC, resulting in different degrees in porosity of HC. Antoran et al., designed a pre-treatment on waste hemp hurd (WHH) via mild chemical activation using potassium carbonate (K_2CO_3) for the synthesis HC method. The synthesis HC showed a significant increase in oxygen-containing functional groups with the highest specific surface area was shown by WHH activated at a mass ratio of 1:4 followed by subsequent pyrolysis at 800 °C (333.5 m^2/g). Despite its relatively large surface area which often causes thick SEI formation, it exhibited an excellent initial coulombic efficiency of 73 % and achieved reversible charge capacities of 267 and 79 mAh/g at 0.03 and 1 A/g, respectively, suggesting that the structure could provide effective diffusion pathways. This material also demonstrated remarkable cyclic stability and rate capability, maintaining 96 % of its capacity after 300 cycles at a current density of 2 A/g. However, the reversible capacity value is not satisfactory as it dropped to below 100 mAh/g. Wang et al., used hazelnut as the biomass precursor to synthesize HC where the hazelnut underwent acid washing before pyrolysis at 1000, 1200, and 1400 °C [55]. The acid-washed hazelnut shell pyrolyzed at 1400 °C demonstrated the highest electrochemical performance where the reversible capacity was maintained at 306 mAh/g after tested for 100 cycles at 20 mA/g.

Heteroatom doping is known for the ability to tune the electronic configuration of HC in order to improve the performance. Wang et al., proposed a pre-oxidation approach and petroleum asphalt modified with polyphosphoric acid as a precursor as the main techniques used to create P-doped hard carbon material [71]. When P elements are doped into hard carbon, the molecular layer structure within the pseudo-graphite domains was deformed. This resulted in an expansion of the graphite layer spacing and an increase in the number of internal closed micropores, improving the matrix's ability to store Na^+ ions. When comparing P-doped hard carbon (PHC-1300) to undoped hard carbon (HC-1300), the former's reversible capacity increased at a rate of 0.05C during the first charge-discharge cycle, from 240.3 mAh/g to 359.9 mAh/g. Song et al., created an ultra-stable SIB anode of three-dimensional N/O co-doped HCs (NOHCs) from poly(aniline co-pyrrole) [72]. Fast diffusion kinetics and highly reversible electrochemical processes were made possible by the integrated strategy of hetero doping and tailored pore structure, according to in-situ Raman and ion diffusion kinetic studies (GITT and CV). The resulting NOHC-2 anode in half -cell showed high rate performance (160.2 mAh/g at 10.0 A/g) and capacity retention (69.8 % after 15,000 cycles). More significantly, the entire cell, which consisted of the Prussian blue cathode and NOHCs anode, produced a substantially good reversible capacity of 205.5 mAh/g at a current density of 0.2 mA/g and good cyclability tested over 300 cycles at 2000 mA/g. Overall, the full cell made up a high-power density of 985.7 W/kg and a high energy density of 97.3 Wh/kg. Aristote et al., probed into the effect of double and triple doping to study their synergistic effect on HC [73]. They examined the electrochemical performances of phosphorus-nitrogen, phosphorus-sulfur, nitrogen-sulfur, and phosphorus-nitrogen-sulfur double and triple-atom HCs produced from camphor wood (Cmph) as anodes for SIBs. The P–N–S–Cmph exhibited exceptional rate performance, good cycling stability, and a high initial coulombic efficiency (ICE) of 70.74 % with a specific capacity of 280 mAh/g at 2000 mA/g after 500 cycles. The synergistic impact of the S, N, and P heteroatom doping expanding the interlayer spacing of the doped-Cmph-HCs, raising the rate of Na^+ intercalation and deintercalation in the HCs, and providing more active sites for Na^+ storage, contributing to the superior performances of the anode materials. Moreover, sulfur and Na^+ could react reversibly, which lowered the surface's irreversible consumption of Na^+.

Table 1 presents an overview of various precursors, the corresponding pre-treatments applied to these precursors, pyrolysis temperatures, electrolytes used, and their impact on the electrochemical performance in both half-cell and full-cell configurations

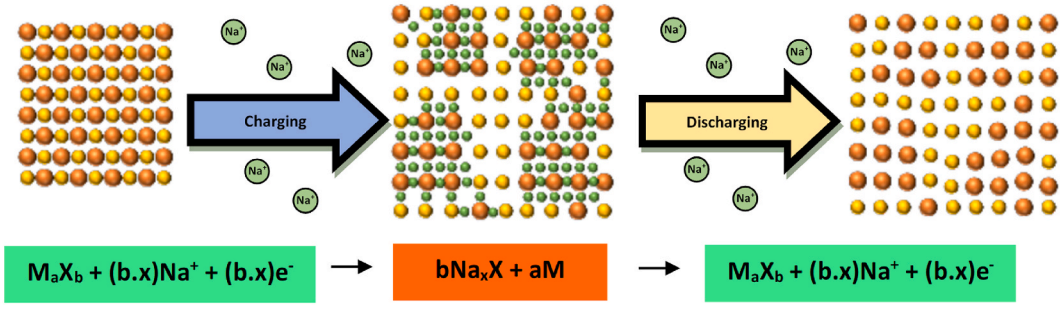

Fig. 7. The conversion reaction and the equation pertaining to the reaction upon charging and discharging process in sodium ion batteries [95].

Table 2
The electrochemical performance of conversion-type anode materials.

Anode Material	Microstructure	Discharge Capacity (mAh/g)	Current Density (mA/g)	Reversible capacity (mAh/g)	Number of Cycles	Capacity retention after the respective cycle (%)	Initial Coulombic Efficiency (%)	Coulombic efficiency (%)	Rate capability (%)	Ref
NiP	Nanosphere	441	50	154	100	54.0	90.0	98.0	441 mAh/g at 50 mA/g; 27.0 mAh/g at 2500 mA/g; 154 mAh/g at 50 mA/g	[101]
NiP@C	Nanosphere wrapped in carbon lamellar	579	50	292	100	75.0	82.0	98.0	579.0 mAh/g at 50 mA/g; 27.1 mAh/g at 2500 mA/g; 452.4 mAh/g at 50 mA/g	
CoP_2	Rod	~300	500	78	1000	31.7	~37.0	~98.0	24 mAh/g at 3000 mA/g	[102]
CoP_2@C	Rod	~1162	500	406	1000	72.1	~56.0	~98.0	272 mAh/g at 3000 mA/g	
MoS_2	Microsphere	560	100	110	100	24.0	N/A	N/A	<100 mAh/g at 1000 mA/g	[103]
MoS_2/C	Microsphere	665	100	342	100	~70.0	77.9	98.0	102 mAh/g at 1000 mA/g	
$CoSe_2$@C	Nanofiber	~510	100	~50	29	~13.8	N/A	~96.0	N/A	[104]
CoSe@BCN-750	Nanobud	926	100	580	100	~98.0	68.5	~96.0	338 mAh/g at 2000 mA/g	
		~420	8000	~210	4000	96.0	~85	~99.0		
$CoSe_2$/NC	Sphere	548.8	200	375.5	200	~78.0	85.3	~99.0	N/A	[105]
		N/A	5000	294.5	1800	N/A	N/A	99.0		
$CoSe_2$/NC@NCNTs	Peapod-like nanorod	554.4	200	473.1	200	~94.0	90.2	~99.0	473.4 mAh/g at 0.2 A/g; 386.3 mAh/g at 10.0 A/g; ~450 mAh/g at 0.2 A/g	
		~410	5000	394.2	4500	N/A	N/A	98.0		
$FeSe_2$@C	Nanorod	624	500	255	160	~62.0	67.0	~98.0	N/A	[106]
$FeSe_2$@C/NG	Nanorod wrapped in graphene layer	603	500	411	160	~82.0	70.0	~98.0	456 mAh/g at 0.2 A/g; 291 mAh/g at 7.0 A/g; 469 mAh/g at 0.2 A/g	
H–$MoSe_2$/NC	Nanotubes	561	1000	429	150	98.0	77	99.0	475 mAh/g at 0.2 A/g; 236 mAh/g at 10.0 A/g; 475 mAh/g at 0.2 A/g	[107]
$MoSe_2$/HCNS	Nanosheets in carbon nanosphere	~920	1000	502	1000	~87.0	~65.0	~98.0	562 mAh/g at 1 A/g; 382 mAh/g at 10 A/g; 532 mAh/g at 1 A/g	[108]
		~680	3000	471	1000	~96.0	~72.0	~98.0		
M-FeS@C + CNT	Platelet	~436	1000	~366	860	89.3	~95.0	98.9	505 mAh/g at 50 mA/g; 332 mAh/g at 10 A/g	[109]
CoWSe/NCP	Polyhedron	~650	1000	434.9	5000	~95.0	~99.0	~99.0	579 mAh/g at 0.1 A/g; 339.6 mAh/g at 20 A/g	[99]
Fe_2O_3.C-CF	Spherical	1154	30	533	100	70.0	82.0	N/A	1050 mAh/g at 30 mA/g; 96 mAh/g at 1 A/g; 575 mAh/g at 30 mAh/g	[110]

within sodium-ion battery systems. Based on the table it could be summarized that the synthesis of hard carbon for various applications in energy storage, particularly in sodium-ion batteries, encompasses several strategies each with distinct advantages and challenges. One step pyrolysis stands out in terms of cost-effectiveness and utilization of renewable resources, yet achieving consistent quality can be challenging due to variations in feedstock and pyrolysis conditions. Hydrothermal method which offers simplicity and environmental friendliness, utilizes water or other solutions as the medium at relatively low temperatures and pressures. However, its long reaction times and potential for low carbon yield pose limitations in controlling morphology and properties. Chemical activation enhances pore structure and surface area, leading to improved electrochemical performance, but concerns arise regarding the use of corrosive chemicals and high temperatures, potentially increasing production costs and environmental impact. Template-assisted synthesis provides precise control over morphology and structure, yielding materials with tailored pore size and distribution, but may require additional steps for template removal and scalability challenges. In terms of electrochemical performance, chemical activation and template-assisted synthesis might have emerged as promising methods due to their ability to produce hard carbon with high surface area and porosity. However, the cost-effectiveness and industrialization feasibility of these methods must be carefully evaluated, with pyrolysis of biomass offering potential as a cost-effective and sustainable alternative. Ultimately, the selection of the best synthesis method should balance performance, cost, and scalability to meet the demands of industrial applications effectively which are subject to the type of precursors used since the resultant product are often affected by their precursor composition.

2.1.2. Graphite

Graphite is an allotrope of carbon of graphene layers whereby each layer is composed of 6 carbon atoms arranged in sp2 hybridization forming honeycomb-like lattice and the gap between atoms is 0.14 nm. Each layer is separated within 0.34 nm and bonded through van der Waals interactions. Its conductive properties stem from the delocalized electrons that move in planar direction. While this graphite interspacing layer works well with the insertion of small Li ions with a high theoretical reversible capability (372 mAh/g), there are some limitations using Na ions. For Na ions to properly insert into the graphite layers, the minimum distance of 0.37 nm is required in comparison to that of pristine graphite [30] which could be achieved by increasing the distance of graphite interspacing layer.

In LIBs, the Li ion successfully intercalated in graphite anode is called graphite intercalated compound (GIC), Li_xC_6 ($0 \leq x \leq 1$), which is the main compound. However, the weak Na + -graphene cation-π interaction can hamper the Na + storage in graphite, namely Na_xC ($x \ll 0$), and no stable Na–C binary compounds such as NaC_6 have been identified so far. Although is often associated with

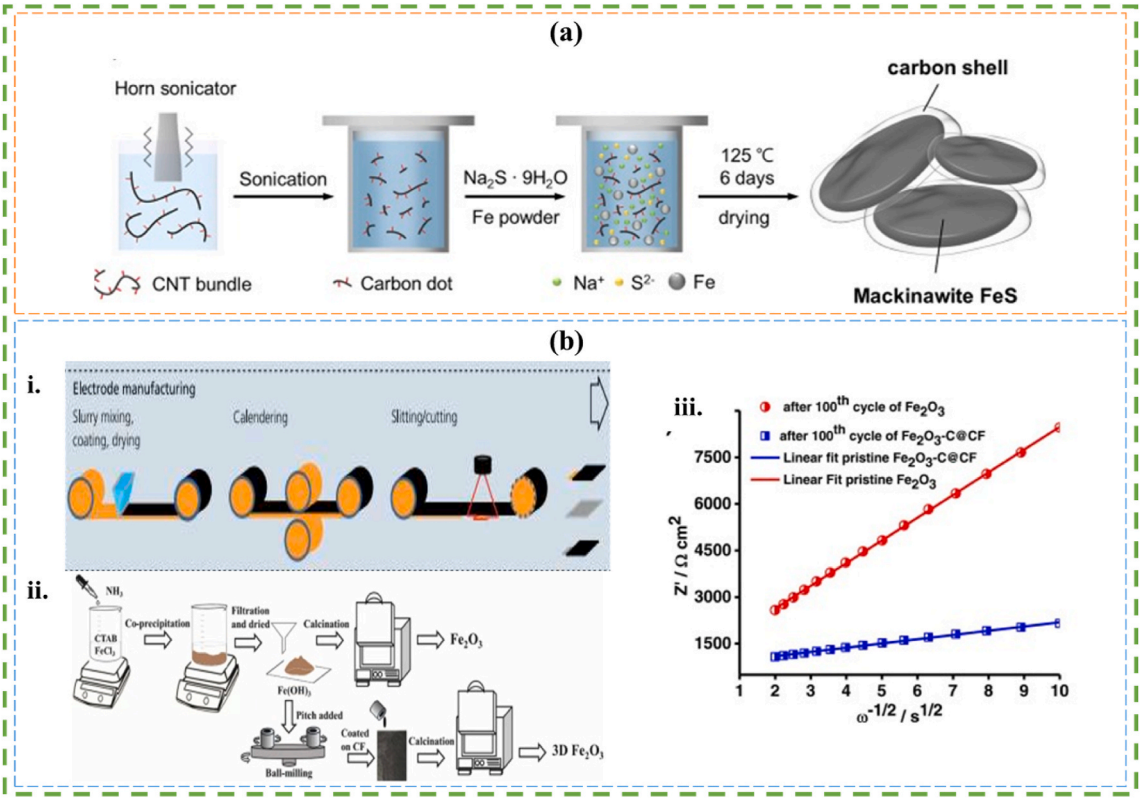

Fig. 8. (a) The one-step hydrothermal reaction to synthesize carbon shell-coated mackinawite FeS platelet [109] and (b)i. Conventional method of fabricating anodes in metal-ion batteries (Agarwal et al., 2015), (b)ii. fabrication of freestanding Fe_2O_3.C-CF anode, Na^+ ions diffusion coefficient of Fe_2O_3.C-CF and Fe_2O_3 anodes acquired from EIS plot [110]. Reproduced with permission. Copyright 2023 Elsevier.

the ionic size, the stability of compound formation is more closely related to the electronegativity of the alkali metal elements, with an exception for Li; the smaller ionic radius going up the periodic table, the weaker the metal-carbon bond which is indicated by the more positive energy formation as expressed in the following equation from which the graphs in Fig. 4 were obtained [79].

$$\Delta E = E_{AM-GIC} - E_{graphite} - E_{AM}$$

For that reason, K ion with larger ionic size is more capable of being intercalated to form K-GIC and reversibly extracted from graphite in K ion batteries (KIBs) [80]. Since the intercalation of Na ion in graphite is rather limited due to the thermodynamic instability in terms of the positive energy formation of the compounds, several methods were adopted on the pristine graphite to facilitate Na ion intercalation into graphitic layers such as modification on pristine graphite to increase the interlayer spacing between graphene layers and Na co-intercalation through solvation process.

It was known that expanded graphite could improve the performance of SIBs after subjected to two-step oxidation-reduction process. The step begins with the oxidation process known as slightly modified Hummer's method followed by the thermal reduction process at relatively high temperature to reduce the oxygen content in the oxidized graphite as illustrated in Fig. 5 [81].

It was found in a recent study that the intercalation in the prepared expanded graphite in the Na-ion battery exhibited the highest initial reversible capacity of 261 mAh/g and maintained high reversible capacity of 100 mAh/g at a current density of 1 A/g after 2600 cycles with an interlayer spacing of 0.40 nm after the thermal reduction of graphite oxide at 600 °C [81]. The condition of final product of expanded graphite could be catered through the temperature of reduction process to change the carbonization degree and disordered structure. The lowest interlayer spacing of 0.38 nm exhibited the lowest performance which agrees with the need for interlayer spacing to be at least 0.37 nm for facile Na-ion intercalation. This finding concurred with the study conducted by David and Singh stating that further reduction in the interlayer spacing subside the performance substantially [82]. Nonetheless, expanded graphite with the presence of oxygen or anion-based pillars could easily react with the electrolyte meanwhile the repulsive force exhibited thereof could hamper the restacking of Na ions in long range order along the c-axis. Therefore, a hierarchical micro-composite called Bi nano/submicron spheres and expanded graphite (H–BiS/EGF) was investigated for the use as anodes for sodium-ion batteries. With the aid of Bi cation to increase the interlayer distance, the expanded graphite exhibited impressive electrochemical performance, including a reversible capacity of 288 mAh/g at 0.5 A/g and outstanding cycle stability (95 % capacity retention for 17300 cycles at 5 A/g) [83].

Besides the well-known expanded graphite or reduced graphite oxide through two-step oxidation reduction method which introduces the anion-based pillar of oxide to allow the better intercalation of Na^+ into their expanded layers, the layers could also be supported through cation-based pillars such as Al and Bi. However, these fillers could be impediment to the intercalation due to the reduction of volume capacity and energy density of electrode materials. Through a ball-milling procedure, the high-defect graphite-type anodes were systematically created, producing extremely defective graphite with a threefold increase in Na^+ storage capacity in comparison to pristine graphite [84]. The capacity of the high defect graphite was found to be 128.7 mAh/g at 0.1 A/g, with a remarkable capacity retention over 8000 cycles at a high current density of 5 A/g. The presence of atomic flaws and smaller particle sizes, as well as the transformation of the hexagonal space group into the rhombohedral space group after ball-milling, are all shown by structural analysis. These modifications lead to increased interlayer spacings and severely warped lattice areas, which improved Na^+ ion adsorption and intercalation. In addition, the difficulty of weak sodium-graphite binding could also be overcome by constructing an activated graphite (AG) material with a large number of defects. This material was able to achieve a stable reversible capacity of 139.1 mAh/g at 1.0 A/g with small capacity decay of 0.0034 % per cycle after 4500 cycles. The effect of defects on graphite was again proven where the high-defect graphite exhibits remarkable capacity retention over 8000 cycles at 5 A/g and a capacity of 128.7 mAh/g at 0.1 A/g.

Another common method to ensure the proper intercalation of Na ions is by solvation of Na in some specific solvents. The solvation of Na^+ ion method was found to lower the energy formation of Na-GIC from 0.03 eV in pristine graphite to −0.87 eV [85]. The assistance of ether-based solvents, graphite could accommodate Na^+ ions and reversibly extract the same [86], and it is a more effective approach as a SIB anode than modifying graphite, for instance through functionalization.

2.1.3. Carbon nanotubes

Carbon nanotubes (CNTs) have been receiving a huge attention as anode materials in SIB owing to the 1D nanostructures, large surface area, high conductivity, remarkable flexibility, and high chemical stability with an interlayer spacing of 0.34 nm. The sodiation occurs in CNTs is also similar to graphite wherein the alkali metal ions intercalate into the interspacing layer of CNTs. However, due to the small d-spacing of MWCNTs, MWCNTs are not preferable to be used as it limits Na^+ ions to properly intercalate into the MWCNTs. This was supported by the report where the reversible capacities showed by MWCNT was merely 82 mAh/g at a current density of 30 mA/g [87].

Altering the structure is seemingly effective to improve the electrochemical performance of SIBs. By partially increasing the interlayer spacing in a few outer layers of multiwalled carbon nanotubes (PECNT) through Hummer's approach, it was reported that PECNT demonstrated a satisfactory cyclic stability over 100 cycles with a specific capacity of 510 mAh/g, which was 2.3 times higher than that of the pristine MWCNT at the same current density of 20 mA/g [88]. In addition, it is also possible to alter the structure of CNT by creating plentiful mesopores, high disorder, and rich flaws in carbon nanotubes (F-CNTs) over an ethanol flame [89]. F-CNTs electrode exhibited a consistent cycling life and a remarkable rate capacity of 145 mAh/g at 1000 mA/g.

As mentioned earlier, the introduction of heteroatoms in carbonaceous materials could alter their electronic activity by improving the electronic and ionic transport of the material. A template-based research was used with polypyrrole as the high nitrogen-containing carbon precursor to produce hollow carbon nanotubes (NCNT) with a long aspect ratio that were N-rich (up to 15.7 %) [90].

Remarkably, NCNT-600 electrode exhibited a good reversible capacity of 132 mAh/g after 5000 cycles for SIBs and 170 mAh/g after 2000 cycles for LIBs at the same current density of at 4000 mA/g. The investigation on the co-effect of the unique hollow nanotube structure and dual N, P doping (NPC) found that the use of NPC yielded exceptional rate performance and long-term cycling stability whereby after 3000 cycles, the NPC electrode might achieve a high reversible capacity of 180.3 mAh/g, even when evaluated at a high current density of 5000 mA/g [91].

2.1.4. Graphene

Graphene and its other graphene counterparts have shown great potential to be applied SIB owing to their unique 2D structures with an outstanding electrical conductivity and large surface area. However, the performance of pristine graphene is still unsatisfactory with relatively low specific capacity since the Na^+ ions intercalate in the same manner as in graphite that are unfavourable thermodynamically along with tendency to restack [92]. Numerous works were presented to enable the integration of graphene to exploit its remarkable properties. One of which is by establishing graphene-based composite with intercalation, conversion, or alloying type anodes.

Apart from being used as the main constituent, graphene could also be incorporated as an additive to the anode material to enhance the performance. Functionalized graphene (FNG) was added to create a petroleum-based mesocarbon microbeads (MCMB) with a loose microcrystalline structure and extremely large size [93]. The findings showed that the increase in FNG could delay the growth of mesophase spheres, prevented coalescence, and impeded the ordered stacking of planar aromatic macromolecules by increasing the interlayer spacing as depicted in TEM images in Fig. 6(a). As a result, the MCMBs with 1.0 wt% FNG provided a competitive specific capacity of 123.4 mAh/g at a current density of 1.0 A/g, a high initial coulombic efficiency of 81.79 %, and excellent cycle performance stability (Fig. 6(b)).

Doping with heteroatom has seemingly become staple as it is proven to improve the electronic properties of carbonaceous materials as anodes in SIBs. A highly doped graphene nanosheets with tunable N and S codopants (NS-GNS) was studied, which were made using a simple one-pot method [94]. Na^+ ions adsorption could occur on the graphene network's surface due to the introduction of in-plane "hole" defects brought about by N-doping, which created a significant amount of space for holding more charges whereas S-doping-induced protrusions into graphene frameworks (Fig. 6(c)) could significantly improve electrochemical performance and allow for the reversible adsorbed/desorbed of Na^+ ions on the external surface. The fast charge storage kinetics were confirmed by electrochemical impedance spectroscopy (EIS) (Fig. 6(d)) where the reduced semi-circle as presented in the inset indicated that the charge-transfer resistance was significantly reduced when heteroatoms were doped into aromatic carbon frameworks. The NS-GNS electrode exhibited a high reversible capacity of approximately 400 mAh/g when it integrates the numerous N, S, and O-induced electrochemical redox centers at varying potentials with the excellent rate capability and exceptionally long cycle life of 10,000 cycles.

In summary, hard carbon (HC), graphite, carbon nanotubes (CNTs), and graphene each possess unique advantages and encounter specific challenges as anode materials in sodium-ion batteries (SIBs). While HC demonstrates high capacity and reversible cycling, challenges persist in controlling its microstructure and optimizing synthesis parameters. Strategies such as engineering pore structures and heteroatom doping hold potential for enhancing its electrochemical properties. Graphite exhibits excellent electrical conductivity but faces limitations in Na + ion intercalation due to its narrow interlayer spacing. Similarly, CNTs offer high conductivity but encounter challenges in Na + ion intercalation and production costs. Likewise, despite its remarkable conductivity, graphene grapples with issues like restacking, low specific capacity, and production costs. Consequently, HC emerges as the most promising carbon-based material owing to its performance, tailorability, and relatively cost-effective production.

2.2. Conversion-type materials

Conversion-type materials (CTM) are the materials that undergo a chemical transformation through diffusion of Li^+ or Na^+ ions with the anode materials to form a new compound that allows the chemical storage energy as presented in Fig. 7 [95], along with the following overall equation.

Where *M* is a transition metal and *X* a non-metal. The reaction of Na^+ ions with the anodes results in the conversion of the anodes of M_aX_b into $Na_bX_x + aM$. The materials that fall under this group include phosphides, oxides, sulfides, and selenides of transition metals and metal-organic framework (MOF) based materials. Besides the benefits of high specific capacity, their production costs are also advantageous from the fact that a large number of CTM exist naturally [96]. However, the CTM anodes critically suffer from large volume variation due to their ability to accommodate high numbers of large Na^+ ions and sluggish reaction kinetic [97,98]. Some of which also possess low electrical conductivity which could affect the rate performance could be a hindrance to obtaining good electrochemical performance. In recent years, engineering heterostructures in metal oxides/sulfides/selenides has gained attention in addressing the aforementioned issues. Heterostructure electrodes generally outperform their individual counterparts as shown in Table 2 due to their synergistic effects in which they integrate component advantages, have smaller band gaps for superior conductivity and charge transfer, exhibit enhanced structural stability and lifespan, and induce more active sites for alkali metal ion adsorption at heterogeneous boundaries. Diversified heterogeneous anodes, such as $CoSe_2$/ZnSe and $SnSe_2$/ZnSe heterostructures, have been employed to augment sodium storage capability [99]. In fact, introducing heteroatoms in the metal/carbon hybrid as dopants could also enhance the performance through the improvement of the electron activation of C. For instance, Pei et al., exploited the advantages of heterojunction engineering for its quick charge transfer by creating a hybrid of $Co_{0.85}Se/WSe_2$ heterostructure with Se vacancies and N-doped carbon polyhedron (CoWSe/NCP) [99]. The vacancies have the ability to significantly increase the Na^+ adsorptionability. The phase interface of the $Co_{0.85}Se/WSe_2$ heterostructure and the presence of Se vacancies are confirmed by spherical aberration-corrected transmission electron microscopy. The CoWSe/NCP anode in sodium-ion batteries outperforms

practically all Co/W-based selenides with an exceptional rate capability (339.6 mAh/g at 20 A/g). Meanwhile, Liang et al., designed an anode with a unique hierarchical nanosphere structure of $Ni_{0.85}Se/MoSe_2$ with its heterointerface surrounded by N-doped carbon to enhance the reversibility with high rate performance ($Ni_{0.85}Se$/(1T-2H)–$MoSe_2$@N–C) [100]. There are numerous phase boundaries in the $Ni_{0.85}Se$/(1T-2H)–$MoSe_2$@N–C anode formed, including 1T-$MoSe_2$/$Ni_{0.85}Se$, 2H–$MoSe_2$/$Ni_{0.85}Se$, and 1T-$MoSe_2$/$Ni_{0.85}Se$, that eventually facilitate quick Na^+ ion diffusion kinetics, and hence exhibiting outstanding reversibility, long cycling performance with superb rate capability (271.7 mAh/g after 2000 cycles at 5.0 A/g with 97.5 % capacity retention). According to the first three GCD curves, the full cell testing using $Na_3V_2(PO_4)_3$@N-CNTs (NVP@N-CNTs) cathode exhibited a high initial charge and discharge specific capacity of 158.7 and 112.0 mAh/g, respectively, in the voltage window of 2.0–4.0 V, yielding the energy densities for the entire cell of 291.3 Wh/kg.

While FeS is commonly studied as cathode material (CTM) anodes in sodium-ion batteries (SIBs), certain phases of FeS remain rarely reported. Lim et al. designed carbon shell-coated mackinawite FeS platelets via a one-step low-temperature hydrothermal method for high-performance SIBs [109]. Traditionally, the synthesis of conversion anodes involves incorporating carbon materials into the process, followed by subsequent carbonization above 450 °C. However, the hydrothermal method (Fig. 8(a)) eliminated the need for high-temperature carbonization. XRD analysis revealed the formation of M − FeS, coupled with Raman analysis showing the presence of carbon. Additionally, Ox-SWCNTs served as the conductive agent instead of carbon black powder, providing an effective electrical network. This led to a significant improvement in reversible specific capacities, with a retention of 89.3 % over 860 cycles at 1 A/g, compared to M-FeS@C, which could withstand only up to 500 cycles.

Essentially, anode materials are usually made in the form of slurries which is coated on substrates, commonly on copper foil, and followed by drying, smoothing by pressing and compressing (calendering), and lastly slitting to make it viable (Fig. 8(b)i). However, recently, a work based on carbon fiber-based freestanding electrode was designated by embedding Fe_2O_3 nanoparticles on the carbon nanofiber (Fe_2O_3.C-CF) (Fig. 2(b)ii) with the objective of successfully mitigating the pulverization and conductivity issues [110]. The precipitation process with surfactant assistance is used to create Fe_2O_3 nanomaterial. Even though the traditional Fe_2O_3 electrode provided 653 mAh/g capacity during the first discharge cycle, it has poor cycling stability. The freestanding electrode, in contrast, has an improved initial capacity of 1154 mAh/g with 70 % capacity retention. In fact, from the slope of the linear plot of EIS analysis in Fig. 2(b)iii, it was observed that Na-ion diffusivity of Fe_2O_3.C-CF was 28 times faster at the 100th cycle as compared to that of Fe_2O_3, proving the viability of freestanding electrodes without the binder.

Table 2 illustrates the overall electrochemical performance of SIBs using various types of conversion-type anode materials. The heterostructures have been proven to exhibit superior performance compared to their individual structures, maintaining stable reversibility capacity even after many cycles. This demonstrates the synergistic effect between the incorporated materials, alleviating the inherent volumetric fluctuation in CTMs. However, despite recent studies showing high capacity with improved cyclability for CTMs, their synthesis can be time-consuming, involving multiple chemicals and steps. Consequently, this could raise production costs and pose challenges for scaling up.

2.3. Alloying-type materials

Alloying mechanism occurs when sodium ions are alloyed with the elements from group 14 and 15 for instance with silicon (Si), germanium (Ge), tin (Sn), antimony (Sb), and P) upon the sodiation reaction to form Na-M intermetallic binary compounds.

Alloying-type anode materials have gained significant attention in the research and development of sodium-ion batteries (SIBs). These materials offer higher theoretical capacities compared to intercalation-type anodes; Si, Ge, Sn, Sb, and P deliver a theoretical capacity of 954, 369, 847, 660, and 2596 mAh/g respectively [111]. Nevertheless, the setback of the alloying type of anode it could suffer from large volume variation and consequently leading to battery capacity fade and mechanical degradation) in addition to sluggish reaction kinetics.

To overcome these challenges, researchers have undertaken a number of different approaches including the incorporation of inactive elements upon the preparation of the alloy materials via electrodeposition techniques. Incorporation of copper (Cu) in Cu_xSb/Ti electrodes have shown promising sodium storage performance [112]. The electrode showed a first reversible capacity of 385.2 mAh/g with a coulombic efficiency of 76.7 % and the reversible capacity remained at 343.5 mAh/g after 150 cycles at a current density of 0.2 A/g. In another investigation, Rong et al., used iron (Fe) as the inactive element in Sb–Fe–P [113]. The analysis of the composites showed that the $Sb_{47}Fe_{39}P_{14}$ electrode had a high desodiation capacity of 431.4 mAh/g at 100 mA/g and retained by 97.8 % of its capacity after 200th cycle. The addition of inactive metals such as Cu and Fe lessens the degradation of the volume variation during charging and discharging and enhances the conductivity of the electrode.

Liu et al., proposed a structural dimensionality reduction strategy through the development of 2D-layer-structured Bi into a quasi-1D structured $NiBi_3$ with improved reaction kinetics and reversibility in order to achieve high-rate and stable cycling performance for Na/K-ion storage [114]. The quasi-1D intermetallic $NiBi_3$ with low formation energy, metallic conductivity, and 3D Na/K-ion diffusion pathways yields exceptional capacity retention of 94.1 % (332 mAh/g) for Na-ion storage after 15,000 cycles which attests to the alleviated volumetric changes problem. The initial coulombic efficiency is also improved to 93.4 % with enhanced capacity retention for K-ion storage.

Another approach is the design and synthesis of novel nanostructures and morphologies of alloy-based anode materials in order to alleviate the large volumetric change of the anodes. For example, the use of hierarchical nanoporous architectures has been shown to improve sodium storage in antimony (Sb)-based anodes where the hierarchical nanoporous Sb with bimodal porosity instead of nanoporous Sb with unimodal porosity increased the quantity of sodium that can be reversibly stored in Sb by about 27 % [115]. Meanwhile, another report stated that Sb-based nanocrystallites produced through the reduction of the industrial Sb white (Sb_2O_3)

exhibited a much stable cyclability with reversible capacity of 423.6 mAh/g at a rate of 2C after 200 cycles whereas both Sb_2O_3 and Sb/Sb_2O_3 showed negligible reversible capacity (<50 mAh/g) [116]. It was also demonstrated that the utilization of nanoparticles of Ge embedded in hierarchical N-doped multichannel carbon fibers (Ge-NMCFs) exhibited a satisfactory discharge capacity of 303 mAh/g (1st cycle) and 160 mAh/g (700th cycle) for SIBs, 1146.7 mAh/g (1st cycle) and 600 mAh/g (500th cycle) for LIBs [117].

The relatively low specific capacity of Ge due to kinetic limitation upon sodiation could also be likely encountered using layered germanium telluride (GeTe) and a GeTe nanocomposite modified by amorphous carbon (GeTe/C) [118]. The materials offered remarkable Na-ion storage properties of GeTe/C, including a high reversible first volumetric capacity of 662 mAh/cm^3, stable capacity retention of 98.5 % even after 100 cycles, and rapid rate capabilities of 704 mAh/cm^3 at 1 C and 630 mAh/cm^3 at 3 C.

The oxygen vacancy-riched tin dioxide (SnO_2) nanoparticles composites with biomass nitrogen-doped carbon microspheres (SNC composite materials) were also investigated as anode materials for sodium-ion batteries (SIBs) and lithium-ion batteries (LIBs) which were anticipated to play a crucial part in enhancing the stress and conductivity of SnO_2, effectively resolving the aforementioned issues [119]. The optimal SNC-2 electrode not only showed excellent electrochemical performance (reversible capacity of 557.1 mAh/g after 50 cycles at 0.05 A/g, high-rate capability of 329.5 mAh/g and reversible capacity of 320 mAh/g after 1000 cycles even at a high current density of 1.0 A/g) in SIBs, but also exhibited superior electrochemical performance in LIBs.

Silicon was also presented with the attempt to study Si as the anode material in SIB which was studied via incorporation of silicon oxycarbides (SiOCs) [120]. The SiOC sample that was calcined at 900 °C demonstrated strong reversible capacity of 160 mAh/g at 25 mA/g after 200 cycles and good rate performance of 62 mAh/g at 800 mA/g when used as an anode in SIBs. [121], revealed that using 2D self-sourced silicon-embedded carbon sheets created without the addition of silicon source demonstrated a specific capacity of 180 mAh/g was achieved at a current density of 100 mA/gb with a capacity retention rate of 94.6 % and a coulomb efficiency of 99.7 % after 1000 cycles.

To sum up, the latest research on alloying-type anode materials for SIBs has focused on addressing the challenges associated with large volume expansion, improving stability and capacity, and understanding the underlying mechanisms. Various approaches, including the design of novel nanostructures, surface modification, and microstructure engineering, have been explored to enhance the performance of alloying-type anodes. Additionally, the use of advanced characterization techniques has provided further insights into the behavior of these materials. Continued research in this field is crucial for the development of high-energy and long-lasting SIBs.

2.4. Organic materials

Organic electrode materials are the materials comprised of four elements namely C, H, O, and N. One of the earliest works conducted by Armand et al., using di-lithium terephthalate and di-lithium *trans*-trans-muconate, two carboxylate group based organic anodes materials has paved the way of exploring the materials with a number of merits that make them promising candidates of viable anode materials [122]. The facile synthesis step and the ability of being derived from biomass makes their utilization economical and environmentally friendly. They are also structurally contrivable as they could be designed according to the desired properties. They also offer advantages in terms of the availability, high sustainability, low propensity for reaction, and the high capacity [123]. Nevertheless, there are two major issues with organic anode materials, and those are low electronic conductivity which could degrade the reaction kinetics and the high solubility of the materials in the electrolyte could be accounted for fast capacity fading.

Luo et al., prepared an organic material with three carboxylate groups attached to a benzene ring (Trisodium 1,2,4-benzenetricarboxylate (TBC)) [124]. The phase of TBC determined by XRD analysis displayed an amorphous structure where the presence of the third carboxylate group in TBC reduced the solubility of TBC in the electrolyte and increased the reaction potential of the anode, and thus improving the cyclic stability and safety of the organic anode. Meanwhile, the intrinsically low electronic conductivity was eventually compensated by the carbon black mixed in the TBC slurry. TBC maintained a reversible capacity of 137 mA/g after 600 cycles, attributed to the prolonged capacity degradation with the rate of 0.0496 % each cycle. TBC provided an initial charge capacity of 195 mAh/g with a pair of charge/discharge plateaus centered at 0.55 V.

Other functional groups could also be introduced to the carboxylate group to modify the electronic properties thereof. For instance, Na-CPN and Na-CPP, two structurally identical compounds containing pyridine distinguished by the location of the N atoms in phenylpyridine were created and utilized as SIB anode materials [125]. Pyridine molecules cause the corresponding molecules they bind with to be high electron affinity, and consequently improving the electronic conductivity of electrode. With a high reversible capacity of 197 mAh/g, Na-CPP was able to hold 99.1 % of its initial value after 350 cycles at 100 mA/g. Moreover, the Na-CPP electrode maintained a capacity rate of 89.9 % even after 1200 cycles at a current density of 5 C. On the other hand, because of its greater polarization, particle size, and charge transport resistance, Na-CPN performed worse in terms of capacity and rate.

The effect of halogen on organic anode was also explored so as to develop improved organic anode materials [126]. synthesized three halogenated carboxylate-based organic anode materials using three different halogen atoms (F, Cl, and Br) [127]. Disodium 2, 5-difluoroterephthalate (DFTP-Na), a fluorinated carboxylate anode, exhibited superior performance compared to other carboxylate anodes containing H, Cl, and Br with long cycle life (300 cycles), high specific capacity (212 mAh/g), and high rate capability (up to 5 A/g). The two F atoms in DFTP decreased the solubility, improved cyclic stability, and interacted with Na^+ during the redox reaction, as demonstrated by the experimental and computational results, resulting in a high-capacity and stable organic anode material in SIBs.

Overall, despite the increasing number of studies on organic materials as anodes in SIBs, extensive research on this material is still required as they are still not comparable to the other types of anodes. Recent advancements in organic electrode materials for sodium-ion batteries have addressed the challenges of using organic materials such as low electronic conductivity and solubility in electrolytes. Strategies including structural modifications and functional group additions have led to improved cyclic stability, safety, and electrochemical performance. These developments highlight the promising potential of organic materials for advancing sodium-ion

battery technology.

3. Challenges and recommendation for HC anode

Sodium-ion batteries (SIBs) show promise for large-scale energy storage applications. As commercialization of SIBs approaches, the development of advanced anodes, especially hard carbon, becomes increasingly urgent but also poses significant challenges. Hard carbon confronts critical issues including low initial Coulombic efficiency (ICE), an unclear sodium storage mechanism, and scalability challenges. In this discussion, we explore these challenges and offer recommendations to overcome them.

1. Low initial Coulombic efficiency (ICE): Hard carbon materials exhibit a low initial Coulombic efficiency (ICE) mainly due to irreversible reactions occurring during the first charge and discharge cycle. These reactions involve the deposition of electrolyte on the electrode surface, forming a solid electrolyte interphase (SEI) membrane, which consumes a significant amount of sodium ions, surface defects, and internal pores over cycling. While high porosity is associated with a high surface area, it is not desirable as it can lead to a higher rate of electrolyte decomposition, resulting in the formation of SEI and consequently, low ICE. Conversely, thin, ionically conductive, conformal, and durable SEIs are crucial for preventing parasitic interactions between the electrolyte and the hard carbon surface, which can impact rate performance and the first cycle coulombic efficiency (CE) due to interface impedance. To enhance ICE and achieve outstanding overall electrochemical performance of HC for SIBs, reducing the specific surface area and defects of hard carbon, as well as closing some pores to minimize irreversible reactions, can be pursued using various precursor materials and methodologies. Understanding the appropriate pre-treatment or post-treatment method, as well as the pyrolysis temperature, is essential based on the biomass precursor, as each precursor possesses its unique starting microstructure that influences the resulting microstructure and porosity. Furthermore, electrolytes also play a crucial role in determining the ICE of HC in SIBs. They serve as carriers for transporting Na^+ ions to and from the HC sites, especially back to the cathode or Na metal. Given that electrolyte decomposition leads to SEI formation, the optimization of electrolyte is imperative in facilitating the formation of thin, ionically conductive SEI layers. Combining these two factors, the formation of the optimum layers might improve the penetration of Na^+ ions, potentially enhancing the ICE associated with HC utilization.
2. Unclear sodium storage mechanism: The sodium storage mechanism in HC remains unclear despite the establishment of several models that have been discussed above. This ambiguity persists due to the diverse microstructures of hard carbon, necessitating further study to elucidate its mechanisms. The comprehension of sodium storage behaviors from morphological engineering, heteroatom doping, and regulation of graphitic structure on HC could be studied through measurements such as cyclic voltammetry (CV) and other common analysis such as in situ measurements of time resolved X-ray diffraction (XRD), time resolved Raman spectroscopy, nuclear magnetic resonance (NMR), and neutron pair distribution function (PDF) analysis to identify mechanisms upon sodiation and desodiation processes. The mechanism could also be further investigated through computational modelling, for instance RMC and DFT calculation.
3. Scalability of HC: The increasing interest in sustainable energy storage solutions highlight the HC's importance as a key enabler for SIBs. However, scalability and cost-effectiveness in HC production remains great challenges, often involving complex processes and costly precursors. Overcoming these challenges drives exploring sustainable and cost-efficient synthesis methods, such as utilizing biomass waste or natural polymers, to reduce production costs and promote environmental sustainability. Successful scalability involves the synthesis method, development of efficient production processes and equipment capable of generating large quantities of HC consistently and cost-effectively. Identifying appropriate methods for synthesizing HC corresponding to different biomass precursors, such as template-assisted methods, and microwave-assisted pyrolysis, is crucial to meet diverse production requirements. In fact, access to abundant and renewable biomass-derived precursors enhances scalability while supporting sustainable manufacturing practices. Efficiency, sustainability, and quality are key factors in scalable synthesis methods, highlighting the need for eco-friendly approaches and rigorous quality control. By improving the production technique, using eco-friendly materials, and staying green without compromising quality, hard carbon production could be scaled up. This makes it easier to use in sodium-ion battery anodes, pushing energy storage technology forward.

Throughout the challenges and recommendations stated above, embracing innovative strategies to enhance the electrochemical performance and fostering eco-friendly approaches, the prospects for HC in SIBs are promising, paving the way for sustainable and cost-effective energy storage solutions with significant societal impact.

4. Conclusion

SIBs have emerged as highly promising alternatives to lithium-ion batteries for the implementation of large-scale energy storage systems. Extensive research has been conducted to develop highly compatible anodes for SIBs to enhance electrochemical performance, making them competitive with LIBs. This review delves into recent studies on anode materials, covering carbon-based, conversion-type, alloying-type, and organic materials. Each anode material exhibits distinct mechanisms for storing Na^+ ions during charging and discharging.

Throughout the review, it becomes apparent that hard carbon (HC) has garnered significant attention due to its precursor variability, cost-effectiveness, and environmentally friendly characteristics. Even when utilizing biomass as a precursor for HC, leading to cost-effective materials, the electrochemical performance such as sodium working potential, cycling stability, and initial Coulombic efficiency matches other anode materials using more expensive chemical precursors. Furthermore, the amorphous nature of HC

structures results in unique storage mechanisms, categorized into six types. This phenomenon allows for the tunability of HC, achieving high electrochemical performance suitable for practical device applications.

Optimization on the HC synthesis to attain remarkable electrochemical performance could be conducted by using different precursors, as mentioned earlier, where as in the review it could be concluded that synthetic materials generally require higher temperature in comparison with the precursor from biomass wastes. In view of that, biomasses are preferable as the sources are readily available accompanied by the variation of microstructures.

The optimization could also be extended to the parameters involved upon the synthesis process. As such, different pre-treatments namely hydrothermal, template-assisted, and field-assisted sintering could be utilized prior to pyrolysis as they could vary the microstructure of resultant product accordingly.

CRediT authorship contribution statement

Farah Nabilah Shafiee: Resources, Writing – review & editing, Writing – original draft, Investigation, Conceptualization. **Siti Aminah Mohd Noor:** Writing – review & editing, Supervision, Conceptualization. **Muhammad Amirul Aizat Mohd Abdah:** Writing – review & editing, Conceptualization. **Siti Hasnawati Jamal:** Supervision, Resources. **Alinda Samsuri:** Supervision, Resources.

Declaration of competing interest

The authors declare the following financial interests/personal relationships which may be considered as potential competing interests:Siti Aminah Mohd Noor reports financial support and administrative support were provided by National Defence University of Malaysia. If there are other authors, they declare that they have no known competing financial interests or personal relationships that could have appeared to influence the work reported in this paper.

Acknowledgement

The authors acknowledge the financial support from Universiti Pertahanan Nasional Malaysia (PS065-UPNM/2023/GPPP/SG/4).

References

[1] B.M. Bang, J.I. Lee, H. Kim, J. Cho, S. Park, High-performance macroporous bulk silicon anodes synthesized by template-free chemical etching, Adv. Energy Mater. 2 (7) (2012) 878–883.
[2] C. Kumar, 5.9 Million Tonnes Lithium Deposits Found in JandK: Why It's Important, The Times of India, 2023, February 10. https://timesofindia.indiatimes.com/india/5-9-million-tonnes-lithium-deposits-found-in-jk-why-its-important/articleshow/97797384.cms?from=mdr.
[3] P. Pathak, V.K. Singh, K. Chabhadiya, Sequential leaching of strategic metals from exhausted LNCM-cathode batteries using oxalic and sulfuric acid lixiviants, J. Occup. Med. 73 (2021) 1386–1394.
[4] B. Makuza, D. Yu, Z. Huang, Q. Tian, X. Guo, Dry grinding-carbonated ultrasound-assisted water leaching of carbothermally reduced lithium-ion battery black mass towards enhanced selective extraction of lithium and recovery of high-value metals, Resour. Conserv. Recycl. 174 (2021) 105784.
[5] S. Ilyas, R.R. Srivastava, V.K. Singh, R. Chi, H. Kim, Recovery of critical metals from spent Li-ion batteries: sequential leaching, precipitation, and cobalt–nickel separation using Cyphos IL104, Waste Manag. 154 (2022) 175–186.
[6] J. Zhang, G. Liang, C. Yang, J. Hu, Y. Chen, C. Wang, A breakthrough method for the recycling of spent lithium-ion batteries without pre-sorting, Green Chem. 23 (21) (2021) 8434–8440.
[7] Y. Liu, H. Yu, Y. Wang, D. Tang, W. Qiu, W. Li, J. Li, Microwave hydrothermal renovating and reassembling spent lithium cobalt oxide for lithium-ion battery, Waste Manag. 143 (2022) 186–194.
[8] M. Cabello, T. Chyrka, R. Klee, M.J. Aragón, X. Bai, P. Lavela, G.M. Vasylchenko, R. Alcántara, J.L. Tirado, G.F. Ortiz, Treasure Na-ion anode from trash coke by adept electrolyte selection, J. Power Sources 347 (2017) 127–135.
[9] T. Chen, B. Ouyang, X. Fan, W. Zhou, W. Liu, K. Liu, Oxide cathodes for sodium-ion batteries: designs, challenges, and perspectives, Carbon Energy 4 (2) (2022) 170–199.
[10] H. Zhang, Y. Gao, X. Liu, L. Zhou, J. Li, Y. Xiao, J. Peng, J. Wang, S.L. Chou, Long-cycle-life cathode materials for sodium-ion batteries toward large-scale energy storage systems, Adv. Energy Mater. (2023) 2300149.
[11] M. Song, C. Wang, D. Du, F. Li, J. Chen, A high-energy-density sodium-ion full battery based on tin anode, Sci. China Chem. 62 (2019) 616–621.
[12] A. Kamiyama, K. Kubota, T. Nakano, S. Fujimura, S. Shiraishi, H. Tsukada, S. Komaba, High-capacity hard carbon synthesized from macroporous phenolic resin for sodium-ion and potassium-ion battery, ACS Appl. Energy Mater. 3 (1) (2019) 135–140.
[13] X. Zhu, X. Jiang, X. Liu, L. Xiao, Y. Cao, A green route to synthesize low-cost and high-performance hard carbon as promising sodium-ion battery anodes from sorghum stalk waste, Green Energy Environ. 2 (3) (2017) 310–315.
[14] A. Björlin, A. Hansson, Y.L. Zhou, Waste-derived Hard Carbon Anode Materials for Sodium-Ion Batteries: the Potential of Using Cardboard as Precursor Material in Sodium-Ion Batteries for Hard Carbon Production in Sweden, 2023.
[15] B. Lu, C. Lin, H. Xiong, C. Zhang, L. Fang, J. Sun, Z. Hu, Y. Wu, X. Fan, G. Li, Q. Wu, Hard-carbon negative electrodes from biomasses for sodium-ion batteries, Molecules 28 (10) (2023) 4027.
[16] N.J. Song, N. Guo, C. Ma, Y. Zhao, W. Li, B. Li, Modulating the graphitic domains and pore structure of corncob-derived hard carbons by pyrolysis to improve sodium storage, Molecules 28 (8) (2023) 3595.
[17] H.S. Nguyen, A. Latz, An effective model for sodium insertion in hard carbons, Phys. Chem. Chem. Phys. 25 (41) (2023) 28196–28204.
[18] M.V. Reddy, G.V. Subba Rao, B.V.R. Chowdari, Metal oxides and oxysalts as anode materials for Li ion batteries, Chem. Rev. 113 (7) (2013) 5364–5457.
[19] M. Anji Reddy, M. Helen, A. Groß, M. Fichtner, H. Euchner, Insight into sodium insertion and the storage mechanism in hard carbon, ACS Energy Lett. 3 (12) (2018) 2851–2857.
[20] J. Wang, L. Xi, C. Peng, X. Song, X. Wan, L. Sun, M. Liu, J. Liu, Recent progress in hard carbon anodes for sodium-ion batteries, Adv. Eng. Mater. (2024) 2302063. https://doi.org/10.1002/adem.202302063.
[21] T.W. Surta, E. Koh, Z. Li, D.B. Fast, X. Ji, P.A. Greaney, M.R. Dolgos, Combining experimental and theoretical techniques to gain an atomic level understanding of the defect binding mechanism in hard carbon anodes for sodium ion batteries, Adv. Energy Mater. 12 (25) (2022) 2200647.
[22] M. Wahid, D. Puthusseri, Y. Gawli, N. Sharma, S. Ogale, Hard carbons for sodium-ion battery anodes: synthetic strategies, material properties, and storage mechanisms, ChemSusChem 11 (3) (2018) 506–526.

[23] T. Perveen, M. Siddiq, N. Shahzad, R. Ihsan, A. Ahmad, M.I. Shahzad, Prospects in anode materials for sodium ion batteries-A review, Renew. Sustain. Energy Rev. 119 (2020) 109549.
[24] D.A. Stevens, J.R. Dahn, High capacity anode materials for rechargeable sodium-ion batteries, J. Electrochem. Soc. 147 (4) (2000) 1271.
[25] D. Alvira, D. Antorán, J.J. Manyà, Plant-derived hard carbon as anode for sodium-ion batteries: a comprehensive review to guide interdisciplinary research, Chem. Eng. J. 447 (2022) 137468.
[26] M. Thompson, Q. Xia, Z. Hu, X.S. Zhao, A review on biomass-derived hard carbon materials for sodium-ion batteries, Materials Advances 2 (18) (2021) 5881–5905.
[27] M.Á. Muñoz-Márquez, D. Saurel, J.L. Gómez-Cámer, M. Casas-Cabanas, E. Castillo-Martínez, T. Rojo, Na-ion batteries for large scale applications: a review on anode materials and solid electrolyte interphase formation, Adv. Energy Mater. 7 (20) (2017) 1700463.
[28] M. Dahbi, M. Kiso, K. Kubota, T. Horiba, T. Chafik, K. Hida, T. Matsuyama, S. Komaba, Synthesis of hard carbon from argan shells for Na-ion batteries, J. Mater. Chem. A 5 (20) (2017) 9917–9928.
[29] S. Cao, Q. Liu, H. Chen, H. Zhu, Y. Liu, A bimetallic induced enhanced 3D electron transport network supported by micro constrain area of balls-in-ball structure used for high performance sodium storage, Chem. Eng. J. (2023) 144277.
[30] Y. Cao, L. Xiao, M.L. Sushko, W. Wang, B. Schwenzer, J. Xiao, Z. Nie, L.V. Saraf, Z. Yang, J. Liu, Sodium ion insertion in hollow carbon nanowires for battery applications, Nano Lett. 12 (7) (2012) 3783–3787.
[31] Nagmani, S. Puravankara, Insights into the plateau capacity dependence on the rate performance and cycling stability of a superior hard carbon microsphere anode for sodium-ion batteries, ACS Appl. Energy Mater. 3 (10) (2020) 10045–10052.
[32] C. Bommier, T.W. Surta, M. Dolgos, X. Ji, New mechanistic insights on Na-ion storage in nongraphitizable carbon, Nano Lett. 15 (9) (2015) 5888–5892.
[33] Z.V. Bobyleva, O.A. Drozhzhin, K.A. Dosaev, A. Kamiyama, S.V. Ryazantsev, S. Komaba, E.V. Antipov, Unveiling pseudocapacitive behavior of hard carbon anode materials for sodium-ion batteries, Electrochim. Acta 354 (2020) 136647.
[34] S. Alvin, D. Yoon, C. Chandra, H.S. Cahyadi, J.H. Park, W. Chang, K.Y. Chung, J. Kim, Revealing sodium ion storage mechanism in hard carbon, Carbon 145 (2019) 67–81.
[35] N. Sun, Z. Guan, Y. Liu, Y. Cao, Q. Zhu, H. Liu, Z. Wang, P. Zhang, B. Xu, Extended "adsorption–insertion" model: a new insight into the sodium storage mechanism of hard carbons, Adv. Energy Mater. 9 (32) (2019) 1901351.
[36] B. Zhang, C.M. Ghimbeu, C. Laberty, C. Vix-Guterl, J.M. Tarascon, Correlation between microstructure and Na storage behavior in hard carbon, Adv. Energy Mater. 6 (1) (2016) 1501588.
[37] A. Gomez-Martin, J. Martinez-Fernandez, M. Ruttert, M. Winter, T. Placke, J. Ramirez-Rico, Correlation of structure and performance of hard carbons as anodes for sodium ion batteries, Chem. Mater. 31 (18) (2019) 7288–7299.
[38] C. Bommier, W. Luo, W.Y. Gao, A. Greaney, S. Ma, X. Ji, Predicting capacity of hard carbon anodes in sodium-ion batteries using porosity measurements, Carbon 76 (2014) 165–174.
[39] H.D. Asfaw, C.W. Tai, M. Valvo, R. Younesi, Facile synthesis of hard carbon microspheres from polyphenols for sodium-ion batteries: insight into local structure and interfacial kinetics, Mater. Today Energy 18 (2020) 100505.
[40] X. Lin, Y. Liu, H. Tan, B. Zhang, Advanced lignin-derived hard carbon for Na-ion batteries and a comparison with Li and K ion storage, Carbon 157 (2020) 316–323.
[41] H. Tonnoir, D. Huo, R.L. Canevesi, V. Fierro, A. Celzard, R. Janot, Tannin-based hard carbons as high-performance anode materials for sodium-ion batteries, Mater. Today Chem. 23 (2022) 100614.
[42] Y. Zou, H. Li, K. Qin, Y. Xia, L. Lin, Y. Qi, W. Chen, Low-cost lignite-derived hard carbon for high-performance sodium-ion storage, J. Mater. Sci. 55 (14) (2020) 5994–6004.
[43] Z.M. Oktay, Y. Onal, T. Depci, S. Altundag, S. Altin, S. Yaşar, E. Altin, Investigation of electrochemical performance of Na-ion batteries by hard carbon anodes produced by biomass of Prunus armeniaca seeds, J. Mater. Sci. Mater. Electron. 34 (20) (2023) 1543.
[44] J.W. Wang, X.H. Liu, S.X. Mao, J.Y. Huang, Microstructural evolution of tin nanoparticles during in situ sodium insertion and extraction, Nano Lett. 12 (11) (2012) 5897–5902.
[45] J. Wang, F. Li, Y. Duan, H. Tao, X. Yang, Sawdust-derived hard carbon as a high-performance anode for sodium-ion batteries, Ionics 29 (6) (2023) 2311–2318.
[46] S. Liu, L. Ge, S. Gao, L. Zhuang, Z. Zhu, H. Wang, Activated carbon derived from bio-waste hemp hurd and retted hemp hurd for CO_2 adsorption, Compos. Commun. 5 (2017) 27–30.
[47] Y. Zhang, R. Remadevi, J.P. Hinestroza, X. Wang, M. Naebe, Transparent ultraviolet (UV)-shielding films made from waste hemp hurd and polyvinyl alcohol (PVA), Polymers 12 (5) (2020) 1190.
[48] S. Momeni, M. Safder, M.A.H. Khondoker, A.L. Elias, Valorization of hemp hurds as bio-sourced additives in PLA-based biocomposites, Polymers 13 (21) (2021) 3786.
[49] M.M. Khattab, Y. Dahman, Production and recovery of poly-3-hydroxybutyrate bioplastics using agro-industrial residues of hemp hurd biomass, Bioproc. Biosyst. Eng. 42 (2019) 1115–1127.
[50] D. Antorán, D. Alvira, M.E. Peker, H. Malón, S. Irusta, V. Sebastián, J.J. Manyà, Waste hemp hurd as a sustainable precursor for affordable and high-rate hard carbon-based anodes in sodium-ion batteries, Energy Fuel. 37 (13) (2023) 9650–9661.
[51] S. Zhang, L. Yue, M. Wang, Y. Feng, Z. Li, J. Mi, SnO_2 nanoparticles confined by N-doped and CNTs-modified carbon fibers as superior anode material for sodium-ion battery, Solid State Ionics 323 (2018) 105–111.
[52] G. Zhang, Y. Zhao, L. Yan, L. Zhang, Z. Shi, Sycamore fruit seed-based hard carbon anode material with high cycle stability for sodium-ion battery, J. Mater. Sci. Mater. Electron. 32 (5) (2021) 5645–5654.
[53] A.A. Arie, B. Tekin, E. Demir, R. Demir-Cakan, Utilization of the Indonesian's spent tea leaves as promising porous hard carbon precursors for anode materials in sodium ion batteries, Waste and biomass valorization 11 (2020) 3121–3131.
[54] X. Ren, S.D. Xu, S. Liu, L. Chen, D. Zhang, L. Qiu, Lath-shaped biomass derived hard carbon as anode materials with super rate capability for sodium-ion batteries, J. Electroanal. Chem. 841 (2019) 63–72.
[55] H. Wang, C. Li, J. An, G. Wang, Biomass derived erythrocyte-like hard carbon as anodes for high performing full sodium-ion batteries, Mater. Sci. Eng., B 286 (2022) 116064.
[56] P. Zheng, J. Sun, H. Liu, R. Wang, C. Liu, Y. Zhao, J. Li, Y. Zheng, X. Rui, Microstructure engineered silicon alloy anodes for lithium-ion batteries: advances and challenges, Batteries and Supercaps 6 (1) (2023) e202200481.
[57] Y. Zheng, Y. Wang, Y. Lu, Y.S. Hu, J. Li, A high-performance sodium-ion battery enhanced by macadamia shell derived hard carbon anode, Nano Energy 39 (2017) 489–498.
[58] Y. Zheng, Y. Lu, X. Qi, Y. Wang, L. Mu, Y. Li, Q. Ma, J. Li, Y.S. Hu, Superior electrochemical performance of sodium-ion full-cell using poplar wood derived hard carbon anode, Energy Storage Mater. 18 (2019) 269–279.
[59] Z. Li, Z. Jian, X. Wang, I.A. Rodríguez-Pérez, C. Bommier, X. Ji, Hard carbon anodes of sodium-ion batteries: undervalued rate capability, Chem. Commun. 53 (17) (2017) 2610–2613.
[60] Q. Wang, X. Zhu, Y. Liu, Y. Fang, X. Zhou, J. Bao, Rice husk-derived hard carbons as high-performance anode materials for sodium-ion batteries, Carbon 127 (2018) 658–666.
[61] M.R. Panda, D.P. Dutta, S. Mitra, Bio-derived mesoporous disordered carbon: an excellent anode in sodium-ion battery and full-cell lab prototype, Carbon 143 (2019) 402–412.
[62] Z.Y. Gu, J.Z. Guo, J.M. Cao, X.T. Wang, X.X. Zhao, X.Y. Zheng, W.H. Li, Z.H. Sun, H.J. Liang, X.L. Wu, An advanced high-entropy fluorophosphate cathode for sodium-ion batteries with increased working voltage and energy density, Adv. Mater. 34 (14) (2022) 2110108.
[63] H.A.H. Ibrahim, Introductory chapter: pyrolysis, in: Recent Advances in Pyrolysis, vol. 1, 2020.

[64] H. Khodaei, L. Gonzalez, S. Chapela, J. Porteiro, P. Nikrityuk, C. Olson, CFD-based coupled multiphase modeling of biochar production using a large-scale pyrolysis plant, Energy 217 (2021) 119325.
[65] N.T.L. Chi, S. Anto, T.S. Ahamed, S.S. Kumar, S. Shanmugam, M.S. Samuel, T. Mathimani, K. Brindhadevi, A. Pugazhendhi, A review on biochar production techniques and biochar based catalyst for biofuel production from algae, Fuel 287 (2021) 119411.
[66] A.L. Pauline, K. Joseph, Hydrothermal carbonization of organic wastes to carbonaceous solid fuel–A review of mechanisms and process parameters, Fuel 279 (2020) 118472.
[67] J. Wang, L. Yan, Q. Ren, L. Fan, F. Zhang, Z. Shi, Facile hydrothermal treatment route of reed straw-derived hard carbon for high performance sodium ion battery, Electrochim. Acta 291 (2018) 188–196.
[68] A. Kamiyama, K. Kubota, D. Igarashi, Y. Youn, Y. Tateyama, H. Ando, K. Gotoh, S. Komaba, MgO-template synthesis of extremely high capacity hard carbon for Na-ion battery, Angew. Chem. Int. Ed. 60 (10) (2021) 5114–5120.
[69] M. Guo, H. Zhang, Z. Huang, W. Li, D. Zhang, C. Gao, F. Gao, P. He, J. Wang, W. Chen, X. Chen, M. Terrones, X. Chen, Y. Wang, Liquid template assisted activation for "egg puff"-like hard carbon toward high sodium storage performance, Small (2023) 2302583.
[70] Y. Zhen, Y. Chen, F. Li, Z. Guo, Z. Hong, M.M. Titirici, Ultrafast synthesis of hard carbon anodes for sodium-ion batteries, Proc. Natl. Acad. Sci. USA 118 (42) (2021) e2111119118.
[71] H. Wang, S. Liu, C. Lei, H. Qiu, W. Jiang, X. Sun, Y. Zhang, W. He, P-doped hard carbon material for anode of sodium ion battery was prepared by using polyphosphoric acid modified petroleum asphalt as precursor, Electrochim. Acta 143812 (2024).
[72] Z. Song, M. Di, S. Chen, Y. Bai, Three-dimensional N/O co-doped hard carbon anode enabled superior stabilities for sodium-ion batteries, Chem. Eng. J. (2023) 144237.
[73] N.T. Aristote, Z. Song, W. Deng, H. Hou, G. Zou, X. Ji, Effect of double and triple-doping of sulfur, nitrogen and phosphorus on the initial coulombic efficiency and rate performance of the biomass derived hard carbon as anode for sodium-ion batteries, J. Power Sources 558 (2023) 232517.
[74] G. Lee, M.E. Lee, S.S. Kim, H.I. Joh, S. Lee, Efficient upcycling of polypropylene-based waste disposable masks into hard carbons for anodes in sodium ion batteries, J. Ind. Eng. Chem. 105 (2022) 268–277.
[75] G. Yasin, M.A. Khan, W.Q. Khan, T. Mehtab, R.M. Korai, X. Lu, M.N. Zahid, Facile and large-scalable synthesis of low cost hard carbon anode for sodium-ion batteries, Results Phys. 14 (2019) 102404.
[76] H.D. Asfaw, R. Gond, A. Kotronia, C.W. Tai, R. Younesi, Bio-derived hard carbon nanosheets with high rate sodium-ion storage characteristics, Sustainable Materials and Technologies 32 (2022) e00407.
[77] E. Canbaz, M. Aydin, R.D. Çakan, Investigation of hazelnut shells driven hard carbons as anode for sodium-ion batteries produced by hydrothermal carbonization method, Turk. J. Chem. 46 (2) (2022) 356–366.
[78] N. Nieto, J. Porte, D. Saurel, L. Djuandhi, N. Sharma, A. Lopez-Urionabarrenechea, V. Palomares, T. Rojo, Use of hydrothermal carbonization to improve the performance of biowaste-derived hard carbons in sodium ion-batteries, ChemSusChem 16 (23) (2023) e202301053.
[79] H. Moriwake, A. Kuwabara, C.A. Fisher, Y. Ikuhara, Why is sodium-intercalated graphite unstable? RSC Adv. 7 (58) (2017) 36550–36554.
[80] X. Li, J. Li, L. Ma, C. Yu, Z. Ji, L. Pan, W. Mai, Graphite anode for potassium ion batteries: current status and perspective, Energy and Environmental Materials 5 (2) (2022) 458–469.
[81] X. Li, Z. Liu, J. Li, H. Lei, W. Zhuo, W. Qin, X. Cai, K.N. Hui, L. Pan, W. Mai, Insights on the mechanism of Na-ion storage in expanded graphite anode, J. Energy Chem. 53 (2021) 56–62.
[82] L. David, G. Singh, Reduced graphene oxide paper electrode: opposing effect of thermal annealing on Li and Na cyclability, J. Phys. Chem. C 118 (49) (2014) 28401–28408.
[83] S. Cai, F. Yan, Y. Zhao, M. Li, Y. Chen, X. He, C. Wang, Hierarchical micro-composite assembled from Bi spheres and expanded graphite flakes as anodes for sodium-ion half/full cells with excellent comprehensive electrochemical performance, Chem. Eng. J. 430 (2022) 132938.
[84] Y. Tian, H. Yang, Y. Zeng, Y. Qi, W. Wang, H. Chen, W. Yin, Y. Ke, Z. Jian, W.H. Kan, W. Chen, Design of high-performance defective graphite-type anodes for sodium-ion batteries, ACS Appl. Energy Mater. 6 (7) (2023) 3854–3861.
[85] G. Yoon, H. Kim, I. Park, K. Kang, Conditions for reversible Na intercalation in graphite: theoretical studies on the interplay among guest ions, solvent, and graphite host, Adv. Energy Mater. 7 (2) (2017) 1601519.
[86] K. Subramanyan, Y.S. Lee, V. Aravindan, Highly promoted solvent-co-intercalation process in pencil graphite anode and $Na_3V_2(PO_4)_3$ cathode in full-cell Na-ion battery, J. Colloid Interface Sci. 632 (2023) 326–334.
[87] X.F. Luo, C.H. Yang, Y.Y. Peng, N.W. Pu, M.D. Ger, C.T. Hsieh, J.K. Chang, Graphene nanosheets, carbon nanotubes, graphite, and activated carbon as anode materials for sodium-ion batteries, J. Mater. Chem. A 3 (19) (2015) 10320–10326.
[88] A.P. Vijaya Kumar Saroja, M. Muruganathan, K. Muthusamy, H. Mizuta, R. Sundara, Enhanced sodium ion storage in interlayer expanded multiwall carbon nanotubes, Nano Lett. 18 (9) (2018) 5688–5696.
[89] W. Han, Y. Zhou, T. Zhu, H. Chu, Combustion synthesis of defect-rich carbon nanotubes as anodes for sodium-ion batteries, Appl. Surf. Sci. 520 (2020) 146317.
[90] S. Zhong, H. Liu, D. Wei, J. Hu, H. Zhang, H. Hou, H. Duan, Long-aspect-ratio N-rich carbon nanotubes as anode material for sodium and lithium ion batteries, Chem. Eng. J. 395 (2020) 125054.
[91] W. Zhong, Q. Chen, F. Yang, W. Liu, G. Li, K. Xie, M. Ren, N, P dual-doped carbon nanotube with superior high-rate sodium storage performance for sodium ion batteries, J. Electroanal. Chem. 850 (2019) 113392.
[92] J. Zhang, W. Lv, Y. Tao, Y.B. He, D.W. Wang, C.H. You, B. Li, F. Kang, Q.H. Yang, Ultrafast high-volumetric sodium storage of folded-graphene electrodes through surface-induced redox reactions, Energy Storage Mater. 1 (2015) 112–118.
[93] Z. Xiang, F. Wang, K. Shi, C. Ye, Z. Fan, G. Liao, J. Liu, Functionalized graphene assisted the formation of mesocarbon microbeads with ultra-large size and loose microcrystalline structure from petroleum pitch for sodium-ion batteries anode, J. Anal. Appl. Pyrol. 175 (2023) 106171.
[94] Y. Ma, Q. Guo, M. Yang, Y. Wang, T. Chen, Q. Chen, H. Xia, Highly doped graphene with multi-dopants for high-capacity and ultrastable sodium-ion batteries, Energy Storage Mater. 13 (2018) 134–141.
[95] B.S. Lee, A review of recent advancements in electrospun anode materials to improve rechargeable lithium battery performance, Polymers 12 (9) (2020) 2035.
[96] P.U. Nzereogu, A.D. Omah, F.I. Ezema, E.I. Iwuoha, A.C. Nwanya, Anode materials for lithium-ion batteries: a review, Applied Surface Science Advances 9 (2022) 100233.
[97] W. Luo, F. Shen, C. Bommier, H. Zhu, X. Ji, L. Hu, Na-ion battery anodes: materials and electrochemistry, Acc. Chem. Res. 49 (2) (2016) 231–240.
[98] H. Kang, Y. Liu, K. Cao, Y. Zhao, L. Jiao, Y. Wang, H. Yuan, Update on anode materials for Na-ion batteries, J. Mater. Chem. A 3 (35) (2015) 17899–17913.
[99] Y.R. Pei, H.Y. Zhou, M. Zhao, J.C. Li, X. Ge, W. Zhang, C.C. Yang, Q. Jiang, High-efficiency sodium storage of $Co_{0.85}Se/WSe_2$ encapsulated in N-doped carbon polyhedron via vacancy and heterojunction engineering, Carbon Energy e374 (2023).
[100] Z. Liang, L. Wang, C. Liu, J. Ouyang, Y. Wu, X. Hao, Self-generated rich phase boundaries of heterostructured $Ni_{0.85}Se$/(1T-2H)-$MoSe_2$@NC hierarchical nanospheres for reversible high-rate sodium-ion storage, Chem. Eng. J. (2024) 148738.
[101] B. Sun, J. Ni, NiP nanoparticles encapsulated in lamellar carbon as high-performance anode materials for sodium-ion batteries, Electrochem. Commun. 141 (2022) 107344.
[102] Z. Hu, M. Tebyetekerwa, A.E. Elkholy, Q. Xia, T. Hussain, H. Liu, X.S. Zhao, Synthesis of carbon-modified cobalt disphosphide as anode for sodium-ion storage, Electrochim. Acta 423 (2022) 140611.
[103] W. Tang, X. Wang, Y. Zhong, D. Xie, X. Zhang, X. Xia, J. Wu, C. Gu, J. Tu, Hierarchical MoS_2/carbon composite microspheres as advanced anodes for lithium/sodium-ion batteries, Chem.–Eur. J. 24 (43) (2018) 11220–11226.
[104] H. Tabassum, C. Zhi, T. Hussain, T. Qiu, W. Aftab, R. Zou, Encapsulating trogtalite $CoSe_2$ nanobuds into BCN nanotubes as high storage capacity sodium ion battery anodes, Adv. Energy Mater. 9 (39) (2019) 1901778.
[105] J. Feng, S.H. Luo, Y.C. Lin, Y. Zhan, S.X. Yan, P.Q. Hou, Q. Wang, Y.H. Zhang, Metal-organic framework derived $CoSe_2$/N-doped carbon core-shell nanoparticles encapsulated in porous N-doped carbon nanotubes as high-performance anodes for sodium-ion batteries, J. Power Sources 535 (2022) 231444.

[106] S.H. Yang, S.K. Park, Y.C. Kang, Metal-organic frameworks derived $FeSe_2$@C nanorods interconnected by N-doped graphene nanosheets as advanced anode materials for Na-ion batteries, Int. J. Energy Res. 45 (15) (2021) 20909–20920.
[107] J.K. Kim, K.E. Lim, W.J. Hwang, Y.C. Kang, S.K. Park, Hierarchical tubular-structured MoSe2 nanosheets/N-doped carbon nanocomposite with enhanced sodium storage properties, ChemSusChem 13 (6) (2020) 1546–1555.
[108] H. Liu, H. Guo, B. Liu, M. Liang, Z. Lv, K.R. Adair, X. Sun, Few-layer $MoSe_2$ nanosheets with expanded (002) planes confined in hollow carbon nanospheres for ultrahigh-performance Na-ion batteries, Adv. Funct. Mater. 28 (19) (2018) 1707480.
[109] H. Lim, S. Kim, J.H. Kim, H.C. Lee, G. Lee, J.H. Park, J.T. Han, K. Cho, Carbon shell-coated mackinawite FeS platelets as anode materials for high-performance sodium-ion batteries, Chem. Eng. J. 458 (2023) 141354.
[110] M. Bhar, S. Ghosh, S.K. Martha, Designing freestanding electrodes with Fe_2O_3-based conversion type anode material for sodium-ion batteries, J. Alloys Compd. 948 (2023) 169670.
[111] L.C. Loaiza, L. Monconduit, V. Seznec, Si and Ge-based anode materials for Li-, Na-, and K-ion batteries: a perspective from structure to electrochemical mechanism, Small 16 (5) (2020) 1905260.
[112] G. Chen, M. Li, Preparation of Cu_xSb/Ti electrodes by electrodeposition and their sodium storage performance, ChemNanoMat 9 (8) (2023) e202300184.
[113] W.Q. Rong, J.H. You, X.M. Zheng, G.P. Tu, S. Tao, P.Y. Zhang, Y.X. Wang, J.T. Li, Electrodeposited binder-free Antimony− Iron− phosphorous composites as advanced anodes for sodium-ion batteries, Chemelectrochem 6 (21) (2019) 5420–5427.
[114] G. Liu, Z. Sun, X. Shi, X. Wang, L. Shao, Y. Liang, X. Lu, J. Liu, Z. Guo, 2D-Layer-Structure Bi to quasi-1D-structure $NiBi_3$: structural dimensionality reduction to superior sodium and potassium ion storage, Adv. Mater. 35 (41) (2023) 2305551.
[115] M. Li, T. Qiu, A. Foucher, J. Fu, Z. Wang, D. Zhang, A.M. Rappe, E.A. Stach, E. Detsi, Impact of hierarchical nanoporous architectures on sodium storage in antimony-based sodium-ion battery anodes, ACS Appl. Energy Mater. 3 (11) (2020) 11231–11241.
[116] Y. Zhu, J. Shao, Y. Jiang, K. Zhang, Q. Shi, Q. Qu, H. Zheng, Sb nanocrystallites derived from industrial antimony white as promising alloying-type anodes for Na-ion batteries, J. Alloys Compd. 926 (2022) 166808.
[117] J. Liu, S. Muhammad, Z. Wei, J. Zhu, X. Duan, Hierarchical N-doping germanium/carbon nanofibers as anode for high-performance lithium-ion and sodium-ion batteries, Nanotechnology 31 (1) (2019) 015402.
[118] G.K. Sung, K.H. Nam, J.H. Choi, C.M. Park, Germanium telluride: layered high-performance anode for sodium-ion batteries, Electrochim. Acta 331 (2020) 135393.
[119] L. Yang, Y. Lei, X. Liang, L. Qu, K. Xu, Y. Hua, J. Feng, SnO_2 nanoparticles composited with biomass N-doped carbon microspheres as low cost, environmentally friendly and high-performance anode material for sodium-ion and lithium-ion batteries, J. Power Sources 547 (2022) 232032.
[120] C. Chandra, J. Kim, Silicon oxycarbide produced from silicone oil for high-performance anode material in sodium ion batteries, Chem. Eng. J. 338 (2018) 126–136.
[121] H. Gong, T. Du, L. Liu, L. Zhou, Y. Wang, H. Jia, Z. Cheng, Self-source silicon embedded in 2D biomass-based carbon sheet as anode material for sodium ion battery, Appl. Surf. Sci. 586 (2022) 152759.
[122] M. Armand, S. Grugeon, H. Vezin, S. Laruelle, P. Ribière, P. Poizot, J.M. Tarascon, Conjugated dicarboxylate anodes for Li-ion batteries, Nat. Mater. 8 (2) (2009) 120–125.
[123] Z. Song, Y. Qian, M.L. Gordin, D. Tang, T. Xu, M. Otani, H. Zhan, H. Zhou, D. Wang, Polyanthraquinone as a reliable organic electrode for stable and fast lithium storage, Angew. Chem. 127 (47) (2015) 14153–14157.
[124] C. Luo, J.J. Shea, J. Huang, A carboxylate group-based organic anode for sustainable and stable sodium ion batteries, J. Power Sources 453 (2020) 227904.
[125] K. Jia, L. Zhu, F. Wu, Phenylpyridine dicarboxylate as highly efficient organic anode for Na-ion batteries, ChemSusChem 14 (15) (2021) 3124–3130.
[126] Y. Huang, X. Li, R. Ding, D. Ying, T. Yan, Y. Huang, C. Tan, X. Sun, P. Gao, E. Liu, Tetragonal MF_2 (M= Ni, Co) micro/nanocrystals anodes for lithium/sodium-ion capacitors, Electrochim. Acta 329 (2020) 135138.
[127] J. Huang, K.I. Callender, K. Qin, M. Girgis, M. Paige, Z. Yang, A.Z. Clayborne, C. Luo, Halogenated carboxylates as organic anodes for stable and sustainable sodium-ion batteries, ACS Appl. Mater. Interfaces 14 (36) (2022) 40784–40792.